

Catalytic residues of microRNA Argonautes play a modest role in microRNA star strand destabilization in *C. elegans*

Kasuen Kotagama^{1,†}, Acadia L. Grimme^{1,2,†}, Leah Braviner³, Bing Yang¹, Rima M. Sakhawala^{1,2}, Guoyun Yu¹, Lars Kristian Benner^{1,4}, Leemor Joshua-Tor³ and Katherine McJunkin^{1,*}

¹Laboratory of Cellular and Developmental Biology, NIDDK Intramural Research Program, 50 South Drive, Bethesda, MD 20892, USA

²Johns Hopkins University Department of Biology, 3400 N. Charles Street, Baltimore, MD 21218, USA

³Cold Spring Harbor Laboratory, One Bungtown Road, Cold Spring Harbor, NY 11724, USA

⁴Current address: Johns Hopkins University Department of Biology, 3400 N. Charles Street, Baltimore, MD 21218, USA

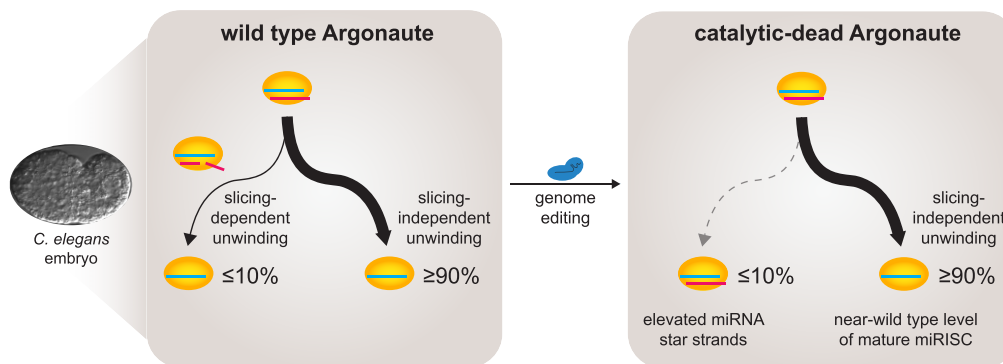
*To whom correspondence should be addressed. Tel: +1 301 496 6991; Fax: +1 301 496 5239; Email: mcjunkin@nih.gov

†The first two authors should be regarded as Joint First Authors.

Abstract

Many microRNA (miRNA)-guided Argonaute proteins can cleave RNA ('slicing'), even though miRNA-mediated target repression is generally cleavage-independent. Here we use *Caenorhabditis elegans* to examine the role of catalytic residues of miRNA Argonautes in organismal development. In contrast to previous work, mutations in presumed catalytic residues did not interfere with development when introduced by CRISPR. We find that unwinding and decay of miRNA star strands is weakly defective in the catalytic residue mutants, with the largest effect observed in embryos. Argonaute-Like Gene 2 (ALG-2) is more dependent on catalytic residues for unwinding than ALG-1. The miRNAs that displayed the greatest (albeit minor) dependence on catalytic residues for unwinding tend to form stable duplexes with their star strand, and in some cases, lowering duplex stability alleviates dependence on catalytic residues. While a few miRNA guide strands are reduced in the mutant background, the basis of this is unclear since changes were not dependent on EBAX-1, an effector of Target-Directed miRNA Degradation (TDMD). Overall, this work defines a role for the catalytic residues of miRNA Argonautes in star strand decay; future work should examine whether this role contributes to the selection pressure to conserve catalytic activity of miRNA Argonautes across the metazoan phylogeny.

Graphical abstract



Introduction

Multiple classes of small RNAs bind to Argonaute proteins to carry out diverse regulatory functions such as post-transcriptional gene regulation, transcriptional regulation, and programmed DNA elimination (1–4). The PIWI domain of Argonaute resembles RNase H and in many Argonautes retains the ability to cleave RNA ('slicing') (4–14). While the role for Argonaute-mediated slicing is well-defined in some small RNA pathways, the role of slicing in the animal microRNA (miRNA) pathway is less clear.

Catalytic activity requires a tetrad of conserved residues (DEDH) (8,9,15,16), with other parts of the protein also contributing supporting roles to catalysis (17–21). The catalytic

or 'slicing' activity of Argonaute proteins can play a role at three phases of the RNA-induced silencing complex (RISC) life cycle: small RNA biogenesis, the unwinding step of RISC assembly, and target RNA cleavage by mature RISC.

The role for slicing in small RNA biogenesis is apparent in multiple small RNA pathways in animals. Slicing by Aubergine (Aub) and Argonaute-3 (Ago3) is required for PIWI-interacting RNA (piRNA) biogenesis in flies (22,23), and slicing activity of Mili is required for piRNA biogenesis in mice (24,25). Notably, *Caenorhabditis elegans* piRNAs (21U RNAs) do not require PIWI slicing activity and instead undergo 5' and 3' trimming of short precursors and subsequent methylation (26–42). In another germline small

Received: January 17, 2023. Revised: February 22, 2024. Editorial Decision: February 23, 2024. Accepted: February 27, 2024

Published by Oxford University Press on behalf of Nucleic Acids Research 2024.

This work is written by (a) US Government employee(s) and is in the public domain in the US.

RNA class, the slicing activity of CSR-1 promotes the RNA-dependent RNA polymerase (RdRP)-dependent biogenesis of CSR-1-bound 22G RNAs (43). Slicing is dispensable for biogenesis of many other classes of small RNAs, including most miRNAs (see below) and many other classes generated by RdRP-dependent modules (1).

In RISC assembly, a small RNA duplex is first loaded into Argonaute. This is followed by unwinding, in which the ‘passenger’ or ‘star’ strand of the duplex dissociates from the complex, leaving the single-stranded ‘guide’ bound to Argonaute as mature RISC. Slicing of the star strand can promote unwinding (12,44–47). The extent to which slicing of the star strand occurs and contributes to unwinding depends on the extent of base-pairing of the small RNA duplex (12,48–50). Thus, star strands of fully complementary siRNA duplexes are efficiently cleaved (12,44–47). In contrast, star strands of bulged miRNA duplexes are generally inefficiently cleaved, and their dissociation is usually slicing-independent (13,51).

In mature RISC, complementary targets occupy the same position as the small RNA star strand and likewise can be cleaved by Argonaute according to similar parameters. RISCs containing the Piwi proteins cleave complementary transposon-derived and genic transcripts in some organisms, while cleavage is dispensable in *C. elegans* (22,52–60). In *C. elegans*, target cleavage by the Argonaute CSR-1 is crucial for regulation of germline and maternal mRNA targets (6,61–68). High complementarity generally promotes target cleavage by slicing-competent Argonautes, but the degree of complementarity required and the efficiency of slicing is guide- and Argonaute-dependent and incompletely understood (12,13,69–73).

In contrast to the clear role for Argonaute-mediated slicing in small RNA biogenesis, RISC assembly, and target cleavage in some animal small RNA pathways, the necessity for slicing in the miRNA pathway is less clear. The catalytic tetrad and slicing activity are conserved in many Argonautes in the miRNA pathway, despite the fact that biogenesis, unwinding, and target repression are slicing-independent for the vast majority of miRNAs. What biological roles does slicing play in the miRNA pathway that maintain selective pressure on the critical catalytic residues?

Biogenesis of animal miRNAs is generally carried out by sequential Microprocessor- and Dicer-mediated cleavage steps (5,74–76), and is generally independent of Argonaute-mediated slicing, with at least one clear exception: miR-451 is generated in a Dicer-independent manner that requires cleavage of its unusual precursor hairpin by Argonaute (77–79). In early *C. elegans* work, elevated miRNA precursors were observed upon RNAi of the miRNA Argonautes (Argonaute-like gene, ALG-1 and -2) (5), and rescue of ALG mutants with catalytic dead overexpression transgenes resulted in upregulation of partially cleaved precursors (13). These results initially suggested a role for ALG-1/2 in general miRNA biogenesis, but this interpretation should be revisited given our current understanding of miRNA biogenesis and more elegant genetic tools (i.e. CRISPR).

Unwinding of animal miRNAs is also largely slicing-independent and is aided by a wedging function of Argonaute’s N domain and residues in the PIWI domain (51,80,81). One exception to this is the miR-486 guide:star duplex which is completely complementary (like an siRNA) and requires Argonaute to cleave the star strand for unwinding and activation of miR-486-RISC (82). Interestingly both

slicing-dependent miRNAs are required for erythropoiesis, and rescuing expression of both miR-451 and miR-486 bypasses the requirement for Ago2-mediated slicing in erythropoiesis (82). Nonetheless, miR-451 and miR-486 are not conserved outside of vertebrates (83), so these described roles for slicing do not explain why miRNA Argonautes would retain their catalytic activity in other animals.

What about target cleavage? In animals, miRNAs generally bind their targets with incomplete complementarity (84–87), which is sufficient for repression of the target through translational repression, deadenylation, and/or decay (88–93), and the vast majority of endogenous miRNA targets are repressed in a GW182-dependent manner that does not require target cleavage, with a few known exceptions (94–104). Because miRISC can efficiently promote target repression in the absence of slicing, slicing may be completely dispensable for target repression, even though it does occur in a limited number of miRNA:target interactions (98–100,102). One complication to answering this question in mammals is the multiple small RNA populations bound by the slicing-competent miRNA Argonaute Ago2. Outside of the vertebrate hematopoietic system, catalytic activity of Ago2 is also required for trophoblast development, a function that is presumed to be due to Ago2’s role in binding endogenous siRNAs (105); Ago2-mediated slicing plays additional as yet unidentified essential roles in intra-embryonic tissues outside the hematopoietic lineage (77,82). In other animals—such as in *C. elegans* and *Drosophila melanogaster*—endo-siRNAs, exo-siRNAs and miRNAs are bound by distinct Argonaute proteins (14,106–114), so conservation of siRNA function would not exert selective pressure on the miRNA Argonautes. The dedicated roles of Argonaute proteins in these systems also makes these models excellent contexts for assessing the roles of slicing in the miRNA pathway.

A study by Bouasker and Simard previously examined the role of slicing in the miRNA pathway in *C. elegans* (13). By rescuing null mutations and RNAi of the miRNA Argonautes with overexpression of catalytically-inactivated Argonautes, Bouasker and Simard observed strong phenotypic effects, suggesting that catalytic activity in the miRNA pathway is important to animal physiology (13). Although small RNAs and mRNAs were not profiled globally, northern blots of select miRNAs showed incomplete precursor cleavage of some miRNAs in the context of overexpression of catalytic-dead Argonaute, suggesting a role for slicing in miRNA biogenesis (5,13).

We set out to revisit the role of the catalytic tetrad in *C. elegans* miRNA Argonautes using CRISPR/Cas9-mediated genome editing and deep sequencing of small RNAs and mRNAs. Here we show that catalytic residues play a role in star strand ejection and decay, and that this is more prominent in the Argonaute ALG-2 than ALG-1. However, the observed effects are only modest when using genome editing to inactivate slicing. A very mild impact on target regulation was observed by RNA-seq. Consistent with this, animal physiology was like wild type. Thus, revisiting this question with state-of-the-art techniques shows that the dramatic effects observed in the previous study may have been due to overexpression (as necessitated by transgenic technologies at that time). This work suggests a modest role for miRNA-guided RNA cleavage in an invertebrate organism. Selective pressure to retain catalytic activity of miRNA Argonautes may be subtle or only apparent in harsher non-laboratory ‘real world’ conditions.

Materials and methods

C. elegans culture

Nematode culture was performed on NGM plates seeded with OP50 (115). Worms were maintained at 20°C except where otherwise noted. Embryo samples were harvested by hypochlorite treatment. For L4 and young adult samples, L1s were hatched overnight in M9 supplemented with cholesterol, then grown on NGM with OP50 for 48 h at 20°C (for L4s) or for 44 h at 25°C (for young adults).

Genome editing

Guide RNAs were designed as close to the site of the edit as possible, while also favoring high GC content and favorable CRISPRscan scores (116,117). Alt-R crRNAs (IDT) were pre-annealed with tracrRNA at 10 μM by heating to 95°C for 5 min in IDT duplex buffer, then cooling to room temperature. Annealed guide RNAs were then assembled with Cas9 (IDT) at 2 μM Cas9 and 4 μM of total guide RNAs. Injection mixes also included donor molecules with 35-nt homology arms for homology-directed repair (118); donor molecules were 100–150 ng/μl (since all donors were relatively short). As a marker of CRISPR efficiency, a guide RNA and donor for *dpy-10* was included in all injection mixes (119).

For *mir-63* and *mir-72* mutations, two rounds of CRISPR were performed. First, the *mir-63* and *mir-72* precursors were deleted and replaced by a cleavage site for an efficient crRNA (120) either in the wild type or the *alg-1(AEDH)*; *alg-2(AEDH)* background (strains MCJ488 and MCJ511). In these backgrounds, CRISPR was performed again to reintroduce the mutant versions of the *mir-63* and *mir-72* precursors.

For 3xFLAG-tagged ALG-2, two rounds of CRISPR were performed. The first generated a deletion near the N terminus of ALG-2 harboring a cleavage site for an efficient crRNA (*cdb12*). This allele was backcrossed twice to N2, then introduced into a background stably expressing Cas9 (oxSi1091); a second round of CRISPR was performed in this strain by injecting crRNA at 1 μM with donor DNA (~100 ng/μl) to restore all deleted sequence while also introducing the 3xFLAG and a short linker sequence in frame (*cdb51*). The resulting locus was then backcrossed twice to N2. To generate the AEDH mutations in the context of 3xFLAG-tagged ALG-1/2, the 3xFLAG-tagged strains of ALG-2 (MCJ133) or ALG-1 (QK67, a gift from John Kim) were injected with CRISPR reagents targeting the first residue of the catalytic tetrad. Strains, alleles and oligos used in this study are listed in [Supplementary Tables S1](#) and [S2](#).

Western blotting

Samples were resuspended by matching worm pellet volume with equal volume 2× lysis buffer and supplementing with additional 1× lysis buffer (30 mM HEPES pH 7.4, 50mM KCl, 0.2% Triton X-100, 2 mM MgCl₂, 10% glycerol, 2 mM DTT, 1× cOmplete, Mini, EDTA-free Protease Inhibitor Cocktail, 1× PhosSTOP phosphatase inhibitor tablets). Samples were lysed by 10 cycles (30 s on, 30 s off) of sonication in a Bioruptor Pico, then clarified by centrifugation at >15 000g for 20 min at 4°C. Samples were quantified by Pierce Reducing Agent Compatible BCA Protein Assay and run on 4–20% TGX gels (Biorad). Membranes were probed with anti-FLAG M2 antibody (Sigma) diluted 1:1000, anti-tubulin DM1A diluted

1:1000 (gift from Kevin O'Connell), anti-H3 1B1B2 diluted 1:1000 (abcam); all hybridizations were carried out in 5% milk in Tris buffered saline with .1% Tween-20.

Brood size assays

Brood size assays were conducted at 25°C after maintaining the strains at 25°C for one generation before the assay. Specifically, MCJ275, MCJ277, MCJ288, N2, RF54 and WM53 strains were grown for ~96 h at 25°C, after which L4 worms were singled onto individual plates. Worms were allowed to grow and lay eggs for 24 h and moved to new plates until the worms stopped laying embryos. Plates with embryos were incubated for another 24 h before larvae and unhatched embryos were counted.

RNAi assays

RNAi plasmids targeting *alg-1* (MSPO171), *alg-2* (MSPO163) and the RNAi control plasmid L4440 were gifted by Martin Simard (13). An RNAi clone targeting the 3'UTR of *alg-2* was gifted by Amy Pasquinelli (121). RNAi plates were prepared with 1 μg/mL IPTG + 1 μg/mL Carbenicillin and stored at 4°C for less than two weeks prior to use. Synchronized L1 populations of worms were generated by alkaline hypochlorite lysis of gravid adults followed by hatching overnight in M9 with 1mM cholesterol at 20°C. (Note that the *gpap-1* SNP is absent from all strains scored in this assay; see also [Supplementary Table S1](#).) Approximately 100 L1 worms were plated on RNAi food or vector control (L4440) and incubated at 15°C for 96h, after which they were scored as fertile adults, dead, slow growing, sterile or males as in (13).

Embryonic lethality assays

Synchronized L1 populations of MCJ275 and N2 worms were generated as described above. L1s were then plated on NGM plates with OP50. Worms were grown at 15°C for 96 h and fertile adults were singled to individual plates and allowed to lay eggs overnight. The following day the adult worms were removed, and the eggs were incubated overnight at 15°C. Larvae and unhatched embryos were counted the next day to evaluate embryonic lethality.

Quantitative miRNA-Taqman

For each sample, 9.96 ng of total RNA was used to perform 5 μl reverse transcription reactions using the TaqMan MicroRNA Reverse Transcription kit (ThermoFisher). After RT, 1.33 μl of 1:4-diluted RT reaction was used in 5 μl qPCR reactions with Taqman miRNA probes and Taqman Universal Mastermix II with UNG (ThermoFisher). Technical triplicates were run for each reaction on the Applied Biosystems QuantStudio Pro 6. Standard curves were generated by similarly performing miRNA-Taqman on a dilution series of an RNA oligo of the sequence of interest (Horizon Discoveries).

Deep sequencing library construction and data analysis

Samples were snap frozen, then resuspended in Trizol and vortexed for 15 min at room temperature. Thereafter, total RNA was purified according to the Trizol manufacturer's instructions (ThermoFisher).

For preparing small RNA libraries, RNA oligos listed in [Supplementary Table S2](#) were spiked into total RNA at a concentration of 1 pg/ μ l in 100 ng/ μ l total RNA. Small RNA libraries were prepared using the NEBNext Small RNA Library Prep kit (NEB), with some modifications. Size selection was only performed after reverse transcription, using 8% urea gels to purify 65–75nt products. RT products were treated with RNase H for 30 min at 37°C prior to gel purification. After excision, products were eluted overnight in 700 μ l 0.3 M NaCl in TE. Products were then purified by isopropanol precipitation, washed in 80% ethanol, and resuspended in 40 μ l 50 mM Tris-HCl 75 mM KCl 3 mM MgCl₂ pH 8.3 before proceeding with the NEBNext protocol. Samples were sequenced on a HiSeq 3000 or NextSeq 550 (Illumina). Raw data can be accessed under SRA Bioproject accession number PRJNA922944.

Small RNA libraries were trimmed using Cutadapt 3.4 (122), then mapped using bowtie2 2.4.4 with settings ‘-no-unal -end-to-end -sensitive’ (123). BAM files were sorted and indexed using samtools 1.13, then assigned to miRNAs using htseq 0.13.5 (124,125). For genome mapping and miRNA assignment, custom reference files were used which included the spiked in RNA oligos. Statistical analysis was performed using DESeq2 and GraphPad Prism (126). For spike-in normalization ([Supplementary Figure S3](#)), size factors for DESeq2 analysis were calculated by dividing spike-in reads in each sample by the median number of spike-in reads per sample. For all other analyses, default DESeq2 normalization was performed using all endogenous miRNA-mapping reads (spike-in reads were excluded from analysis).

For RNAseq, libraries were prepared by Psoimagen using the Truseq Stranded Total RNA Library Prep Kit and sequenced on a NovaSeq6000 S4 (Illumina). Low quality bases and adaptors were trimmed from sequence reads using Cutadapt v2.7 with parameters ‘-q 20 -minimum-length 25’ (122). Resulting reads were mapped to WS277 using HISAT2 v2.1.0 with default parameters (127). Aligned reads were counted using subread featureCounts v1.6.4 with default parameters, except that ‘-s’ option was used to specify appropriate strands (128). Differential expression analysis was done with DESeq2 v1.22.1 (ref4) in v3.5.1 R version (126).

To calculate predicted miRNA:star duplex structures and calculate minimum free energy (MFE), RNAcofold was used with default parameters, as part of the ViennaRNA package (version 2.4.18).

Reagents

The following reagents were used: Alt-R crRNAs (IDT), Cas9 (IDT), Trizol (ThermoFisher), TaqMan MicroRNA Reverse Transcription kit (ThermoFisher), Taqman miRNA probes (ThermoFisher), Taqman Universal Mastermix II with UNG (ThermoFisher), NEBNext Small RNA Library Prep kit (NEB), RNA oligonucleotides (Horizon Discoveries). The following specialized instruments were used: QuantStudio Pro 6 (Applied Biosystems), HiSeq 3000 (Illumina), NextSeq 550 (Illumina), NovaSeq6000 S4 (Illumina), Bioruptor Pico (Diagenode).

Biological resources

All strains used in the study are listed in [Supplementary Table S1](#).

Statistical analyses

Statistical analysis for deep sequencing datasets was performed using DESeq2 using default settings except when spike-ins were used as noted (126). For analysis of standard data types, the Analysis function in GraphPad Prism was used to select and perform the appropriate statistical test. At least three (in most cases four) replicates of each genotype were used for all experiments.

Data availability/sequence data resources

All deep sequencing raw data can be accessed under SRA Bioproject PRJNA922944.

Data availability/novel programs, software, algorithms

Not applicable.

Web sites/data base referencing

MirGeneDB 2.1 (<https://mirgenedb.org/>), miRBase (<https://www.mirbase.org/>), WormBase (<https://wormbase.org/>).

Results

Mutation of catalytic tetrad in both miRNA Argonautes does not impact physiology

To revisit the role of miRISC-mediated slicing in invertebrates, we used CRISPR/Cas9-mediated genome editing to mutate the DEDH catalytic tetrad to AEDH in the major *C. elegans* miRNA Argonaute, ALG-1 and ALG-2 (Figure 1A). (The germline-specific miRNA Argonaute ALG-5 lacks conservation in any of the positions corresponding to DEDH and therefore likely lacks catalytic activity (Figure 1A).) These AEDH mutations did not affect protein abundance ([Supplementary Figure S1](#)). This mutation has previously been shown to completely inactivate catalytic activity in orthologous Argonautes *in vitro* and *in vivo* (9,77). Although the molecular phenotypes presented below are consistent with a slicing defect, a caveat to interpretation of this study is that we have not validated slicing activity of these variants of ALG-1 and -2 directly in slicing assays (see also Discussion).

Mutant strains were superficially wild type. Negligible lethality was observed. Brood size assays showed that single *alg-1(AEDH)* or *alg-2(AEDH)* or double *alg-1(AEDH); alg-2(AEDH)* mutants all had wild-type like fecundity (Figure 1B). In comparison, *alg-1(null)* animals had compromised fecundity, as previously observed (5,129). Therefore, *alg-1(AEDH)* and *alg-2(AEDH)* largely retain wild type function and do not mimic loss-of-function alleles.

These results are in contrast to a previous study in which catalytic dead versions of Argonaute were over-expressed in an Argonaute loss-of-function background (13). In that case, catalytic-dead versions of Argonaute only partially rescued viability and provided no rescue of fertility (all animals were dead or sterile). To more directly compare the phenotypes of the *alg-1(AEDH)* and *alg-2(AEDH)* CRISPR strains to the strains in the Bouasker and Simard study, we performed identical RNAi assays. In these assays, *alg-1* RNAi was performed on wild type, *alg-2(null)* and *alg-2(AEDH)*. Likewise, *alg-2* RNAi was performed on wild type, *alg-1(null)* and *alg-1(AEDH)*. The vector control and *alg-1* and *alg-2* CDS RNAi clones used in Bouasker, et al. were used, as well as an addi-

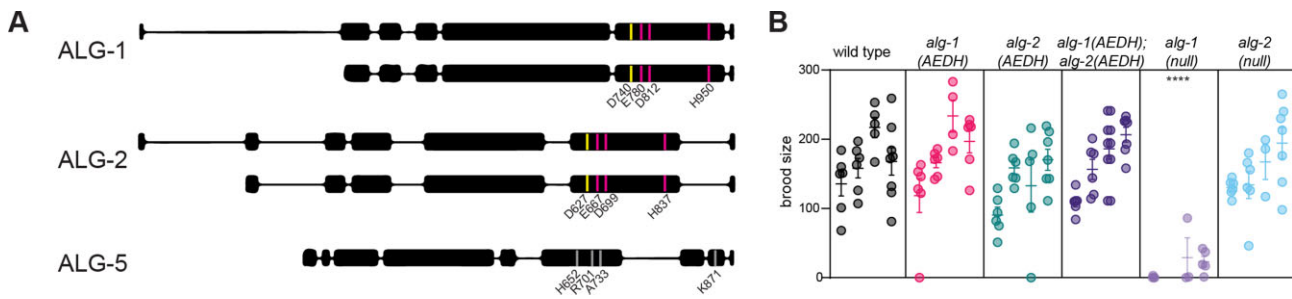


Figure 1. Mutation of catalytic tetrad in both miRNA Argonautes does not impact physiology. **(A)** Schematic of miRNA Argonaute genes in *C. elegans* with positions encoding residues of catalytic tetrad in ALG-1 and ALG-2 highlighted. ALG-5 residues in equivalent positions are not conserved. For ALG-1/2, positions in short isoform are denoted. Yellow position highlights aspartate that is mutated to alanine in 'AEDH' mutants. **(B)** Fecundity assay. Each dot represents one brood; four replicates conducted shown side by side for each genotype. (Only three replicates were done for *alg-1(null)*.) All mutants were compared to wild type by one-way ANOVA with Dunnett's test. Only *alg-1(null)* shows significant difference from wild type. **** $P < 0.0001$. Assay was performed at 25°C.

tional *alg-2* RNAi clone that targets the *alg-2* 3'UTR for enhanced specificity (121). ALG-1 and -2 function largely redundantly (5); thus, as expected, RNAi of the other ALG paralog caused sterility and lethality in the *alg-1(null)* and *alg-2(null)* backgrounds (Supplementary Figure S2). However, RNAi of the other ALG paralog did not induce lethal or sick phenotypes in the *alg-1(AEDH)* or *alg-2(AEDH)* backgrounds (Supplementary Figure S2). Thus, consistent with the wild-type like phenotype of the *alg-1(AEDH); alg-2(AEDH)* double mutant, *alg-1(AEDH)* and *alg-2(AEDH)* do not behave as loss of function alleles in this assay. Taken together, this suggests that the previous study was impacted by expression level of the catalytic dead Argonaute and that, in fact, the catalytic tetrad is not required for grossly normal physiology and fitness.

Some miRNA star strands are slightly elevated in the absence of slicing

Previous work in other models showed that the catalytic activity of Argonaute in the miRNA pathway is crucial for the biogenesis of a Dicer-independent miRNA and the proper loading of an siRNA-like miRNA (77,78,82). To determine the impact of mutating Argonautes' catalytic residues on *C. elegans* miRNAs, we profiled miRNA star and guide strands from embryos, L4 stage larvae and young adults. We chose to profile these stages because of prominent roles of miRNAs in these stages and the differential expression of the miRNA Argonautes across these stages (121,129,130).

Exogenous RNA oligos were spiked in prior to library prep to control for potential large-scale changes in miRNA populations. Spike-in normalization (Supplementary Figure S3) and normalization to all endogenous miRNA reads (Figure 2) yielded similar results, demonstrating that wholesale changes in small RNA population did not occur. Normalization to all endogenous miRNAs resulted in slightly lower variance across replicates and thus yielded slightly more significantly altered small RNAs (Supplementary Figure S3 and Figure 2); thus, we proceeded with this type of normalization for all other analyses.

Embryo samples showed the greatest number of significantly altered miRNAs. Twenty-six miRNA strands were upregulated, all of which are miRNA star strands (Figure 2A, Supplementary Tables S3–S5). Subtle star strand upregulation was also widespread such that star strands were upregulated overall compared to miRNA guide strands in em-

bryos (Figure 2B, C). Ten and six star strands were also upregulated in L4 larvae and adults, respectively (Figure 2A, Supplementary Tables S6 and S7). Changes in miRNA abundance were further validated by Taqman qRT-PCR for a select set of miRNAs (Supplementary Figure S4). The upregulation of star strands suggests that the catalytic residues promote unwinding, as previously observed for siRNAs (12,44–46). The amplitude of these changes is modest compared to the guide:star strand ratio, which is ≥ 10 -fold for most miRNAs (131). Therefore, the putative slicing-dependent unwinding of these star strands occurs alongside a more dominant slicing-independent pathway. This low amplitude of star strand elevation suggests that only a very small proportion of miRNA guide strand function would be impaired and may not result in observable guide strand loss-of-function. Few miRNAs were also downregulated (Figure 2, Supplementary Tables S5–S7). These were mostly miRNA guide strands, including *mir-243-3p*, *mir-1821-3p* and *mir-1829a-5p*, which were each downregulated in more than one developmental stage. Again, the amplitude of changes is modest, suggesting that slicing is not strictly required for the biogenesis of these miRNAs (Figure 2). The mechanism of the downregulation of these guide strands is not understood, though one possible model is explored below.

The contribution of catalytic residues to star strand unwinding may predict that embryos would be more vulnerable to mutations in these residues when grown at low temperature, where increased duplex stability may favor slicing-dependent unwinding (50). We tested this by growing animals at 15°C starting at L1 and scoring hatching rate of their progeny. The viability of the *alg-1(AEDH); alg-2(AEDH)* embryos (99.7%, $n = 364$) was similar to that of wild type (99.4%, $n = 360$). Thus, growth at mild low temperature does not reveal severe phenotypes of the *alg-1(AEDH); alg-2(AEDH)* background. Future work should examine more acute cold shock paradigms as a setting in which catalytic residues may play a more prominent role.

Catalytic residues play a greater role in ALG-2 unwinding than that of ALG-1

We sought to understand why embryo samples displayed more widespread elevation of star strands upon mutation of catalytic residues than other stages. We hypothesized that the larger effect in embryos might be due to a difference in

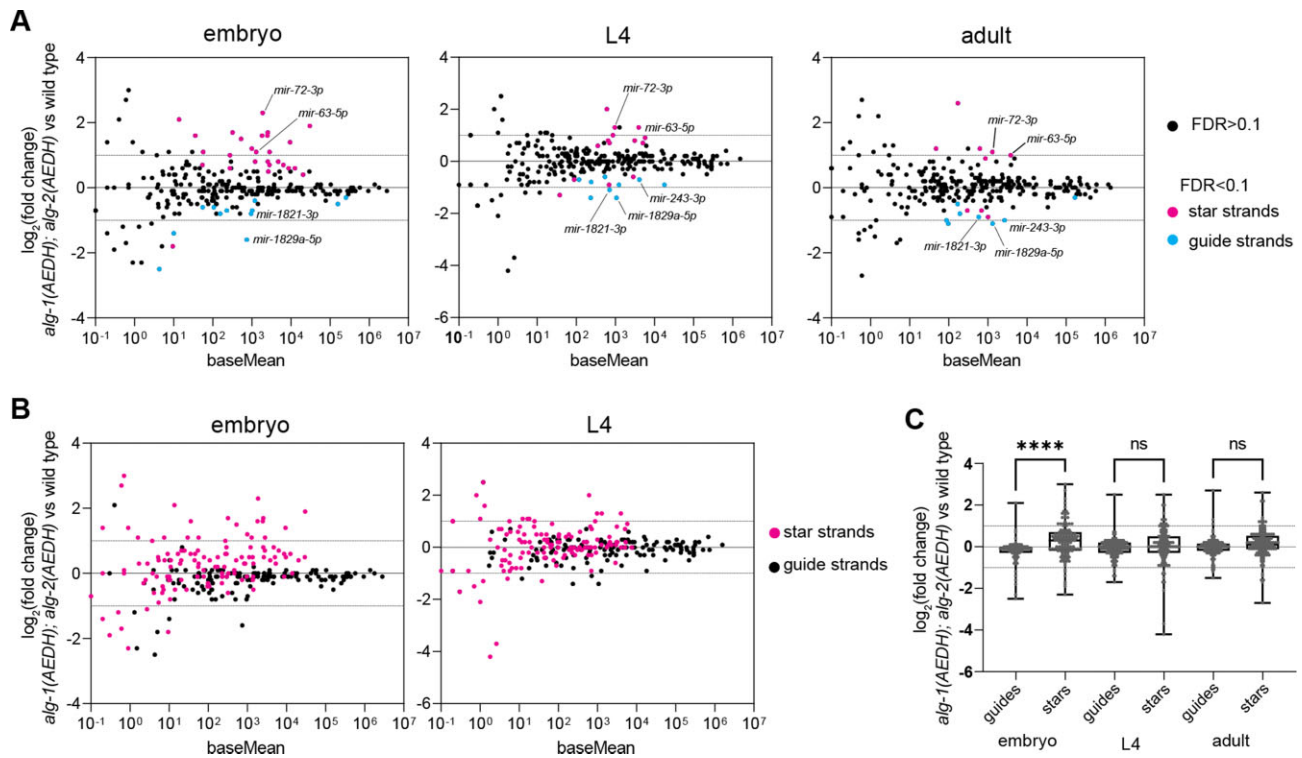


Figure 2. Some miRNA star strands are slightly elevated in catalytic residue mutants. **(A)** MA plot showing average abundance on X-axis and $\log_2(\text{fold change})$ on Y-axis. miRNAs showing significant changes in *alg-1(AEDH)*; *alg-2(AEDH)* versus wild type are shown in blue (miRNA guide strands) or pink (star strands) (DESeq2 FDR < 0.1). Three (L4) or four (embryo and young adult) biological replicates of each genotype were analyzed. **(B)** MA plot as in (A), with all guide strands FDR shown in black and all star strands in pink. **(C)** Summary of $\log_2(\text{fold change})$ values for all guides or star strands in each stage in *alg-1(AEDH)*; *alg-2(AEDH)* versus wild type. $\log_2(\text{fold change})$ of star strands were compared to those of guide strands in the same sample by one-way ANOVA followed by Sidak's multiple comparisons test. **** $P < 0.0001$.

relative expression of the Argonaute paralogs ALG-1 and ALG-2. ALG-2 is expressed earlier in embryogenesis than ALG-1, and its expression decreases after embryogenesis (129,130). Furthermore, the most abundant embryonic miRNA family, *mir-35-42*, largely depends on ALG-2 expression for its stabilization (100,129,132). Together these data suggest that the ratio of ALG-2:ALG-1 is higher in embryos than later stages. Therefore, the larger effect of catalytic residue mutations in embryos may be due to a greater dependence of ALG-2 unwinding on catalytic residues than that of ALG-1.

To test this hypothesis, we profiled small RNAs from embryos that were single mutants, with catalytic residues mutated in either ALG-1 or ALG-2. Single *alg-1(AEDH)* mutant embryos displayed very few significant changes in miRNA abundance (Figure 3A, Supplementary Table S8). In contrast, *alg-2(AEDH)* single mutants showed nearly as many significant changes as *alg-1(AEDH)*; *alg-2(AEDH)* double mutant embryos (Figure 3A, Supplementary Table S9). Below the threshold of significance, star strands were globally slightly elevated in the *alg-2(AEDH)* single mutants, again mimicking the *alg-1(AEDH)*; *alg-2(AEDH)* double mutant (Figure 3B). Therefore, the elevation of star strands in *alg-1(AEDH)*; *alg-2(AEDH)* is largely due to the sensitivity of ALG-2 to catalytic residue mutation. Samples harvested from later stages may show subtler changes in miRNA abundance due to a higher ratio of ALG-1:ALG-2 expression coupled with a lower sensitivity of ALG-1 to catalytic residue mutation.

High duplex stability favors a greater role for catalytic residues in unwinding

While many miRNA star strands were elevated in embryos, very few were elevated in adults and L4, and these were largely consistent across both stages. We further examined the properties of these guide:star duplexes to determine if any distinctive feature might predict the extent to which a miRNA duplex depends on catalytic residues for unwinding.

The star strands *mir-63-5p* and *mir-72-3p* were upregulated across all three stages examined. We observed that *mir-63* and *mir-72* both had relatively low minimum free energy (MFE) of the guide:star duplex compared to other miRNAs (they are both in the lowest 15% of MFEs across all miRNA duplexes) (Figure 4A, B). We also observed that the guide strands of these duplexes displayed a high rate of 3' end trimming (within the top 12% of all guide strands) (133) (Figure 4A).

One possible model is that the high stability of the guide:star duplex slows slicing-independent unwinding (48,50,134). The presence of the star strand could favor a structural conformation in which the 3' end of the guide strand is not bound by the PAZ domain, leaving it vulnerable to exonucleolytic trimming (135,136). Thus, a longer dwell time of the star strand could lead to higher prevalence of trimmed guide strand molecules. The slow rate of slicing-independent unwinding and thereby long dwell time of the star strand could allow the inefficient slicing-dependent star strand ejection mechanism to play a relatively larger (though still minor) role in miRISC maturation.

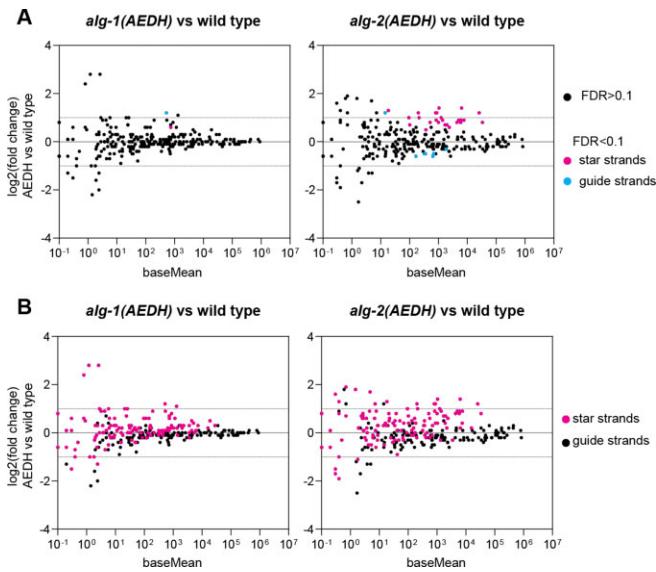


Figure 3. Catalytic tetrad of ALG-2 plays a greater role in star strand destabilization than that of ALG-1. **(A)** MA plot showing average abundance on X-axis and \log_2 (fold change) on Y-axis. miRNAs showing significant changes in *alg-1(AEDH)* or *alg-2(AEDH)* versus wild type embryos are shown in blue (miRNA guide strands) or pink (star strands) (DESeq2 FDR < 0.1). Four biological replicates of each genotype were analyzed. **(B)** MA plot as in (A), with all guide strands shown in black and all star strands in pink.

To test this model, we performed CRISPR to make mutations that are predicted to preserve overall base pairing structure while decreasing duplex stability (i.e. increasing MFE) (Figure 4B). These mutations consisted of one to three mutations on each strand of the miRNA duplex, replacing G:C base pairs with A:U base pairs (Figure 4C). Mutations were introduced near the middle of the duplex (avoiding the terminal four base pairs) in an attempt to preserve thermodynamic asymmetry and strand selection (137–139).

We then examined the mutant duplex miRNAs in an otherwise wild type or the *alg-1(AEDH)*; *alg-2(AEDH)* background to determine whether decreasing duplex stability also reduces the dependence of star strand unwinding on catalytic residues. To measure both star strand stabilization and strand selection, we performed qPCR in L4 samples calibrated with standard curves of synthetic RNA oligos to enable absolute quantification (Supplementary Figure S5). For both wild type *mir-72* and *mir-63*, qPCR confirmed upregulation of the star strand in the *alg-1(AEDH)*; *alg-2(AEDH)* mutant background with no concomitant effect on the guide strand (Figure 4E, F). For *mir-72*, either one or two mutations that reduced thermodynamic stability of the guide:star duplex also abrogated the effect of *alg-1(AEDH)*; *alg-2(AEDH)* on the star strand abundance (Figure 4E). This suggests that the dependence of the wild type duplex on catalytic residues for complete unwinding is due to high thermodynamic stability of the miRNA:star duplex. For both *mir-72* mutant duplexes, the guide strand selection remained high, arguing against an alternative model in which star strand effects are altered by increased star strand loading into Argonaute (Figure 4G).

For *mir-63*, two mutations in the duplex (*mir-63_mut2*) did not abolish the increased star strand abundance observed in the *alg-1(AEDH)*; *alg-2(AEDH)* background (Figure 4F). A third mutation in the duplex of *mir-63* (*mir-63_mut3*) caused

a switch in strand selection that favored loading of *mir-63-5p* over the erstwhile guide strand *mir-63-3p*, making it difficult to interpret the effects of this mutation in the *alg-1(AEDH)*; *alg-2(AEDH)* background (Figure 4H).

Overall, the *mir-72* experiments show that duplex thermodynamic stability is one factor that influences dependence on catalytic residues for unwinding (Figure 4E). At the same time, the weak correlation between thermodynamic stability and dependence on catalytic residues (color and MFE—Figure 4A) and the lack of effect of two mutations in *mir-63* (Figure 4F) together show that other unknown factors also influence dependence on catalytic residues for unwinding.

Minor changes in star strand abundance result in subtle changes in target repression

As discussed above, physiology of the *alg-1(AEDH)*; *alg-2(AEDH)* double mutant animals is grossly normal (Figure 1). Next, we performed RNA-seq to determine whether changes in miRNA abundance (Figure 2) or absence of target cleavage led to a more subtle molecular phenotype. Very minor changes in gene expression were observed. No genes were significantly altered in expression in L4 stage *alg-1(AEDH)*; *alg-2(AEDH)* animals compared to wild type, whereas only one or two were altered in embryo and adult, respectively (Figure 5A, Supplementary Tables S10–S12). These changes were both down-regulation of protein-coding genes (not an up-regulation that might be expected from de-repression of miRNA target genes).

To determine whether indirect effects of miRNA star strand stabilization may more subtly impact gene expression in *alg-1(AEDH)*; *alg-2(AEDH)*, we analyzed all Targetscan-predicted targets of *mir-63* and *mir-72* (140). While no significant effect was observed in embryos or L4s, in adults we observed significant upregulation of predicted targets compared to transcripts not targeted by these two miRNAs; the effect was stronger for *mir-63* targets than *mir-72* targets (Figure 5B). This is consistent with partial loss of function of these miRNAs due to failed maturation of a subset of miRISCs in the catalytic residue mutant. Expression of *mir-63* is highest in adult among the stages examined, which may underlie the stage specificity of this effect, and the low guide:star ratio of *mir-63* in *alg-1(AEDH)*; *alg-2(AEDH)* may underlie the larger effect size for *mir-63* than *mir-72* (Supplementary Figure S6A). Thus, while high-amplitude impacts on individual genes are not observed, the more subtle effects observed by ensemble target analysis are consistent with our model of catalytic residues contributing to star strand unwinding.

We further examined the gene *gpap-1*, which was down-regulated in both embryo and adult *alg-1(AEDH)*; *alg-2(AEDH)* animals (Figure 5A). By close examination of the RNA-seq data, we observed a single-nucleotide polymorphism in the *gpap-1* 5' UTR in *alg-1(AEDH)*; *alg-2(AEDH)* samples (Supplementary Figure S6B). Thus, this polymorphism is very likely the basis of these gene expression changes, rather than the mutations in *alg-1* and *alg-2*. No homology was observed between the guide RNAs used to generate the *alg-1* and *alg-2* alleles and the region containing the SNP in *gpap-1*. Thus, we posit that this SNP is due to genetic drift and fixation that occurred during the generation of the *alg-1(AEDH)*; *alg-2(AEDH)* strain. Overall, this suggests that target mRNA cleavage plays little or no role in regulation of gene expression by miRNAs in *C. elegans*. Furthermore, the role that catalytic

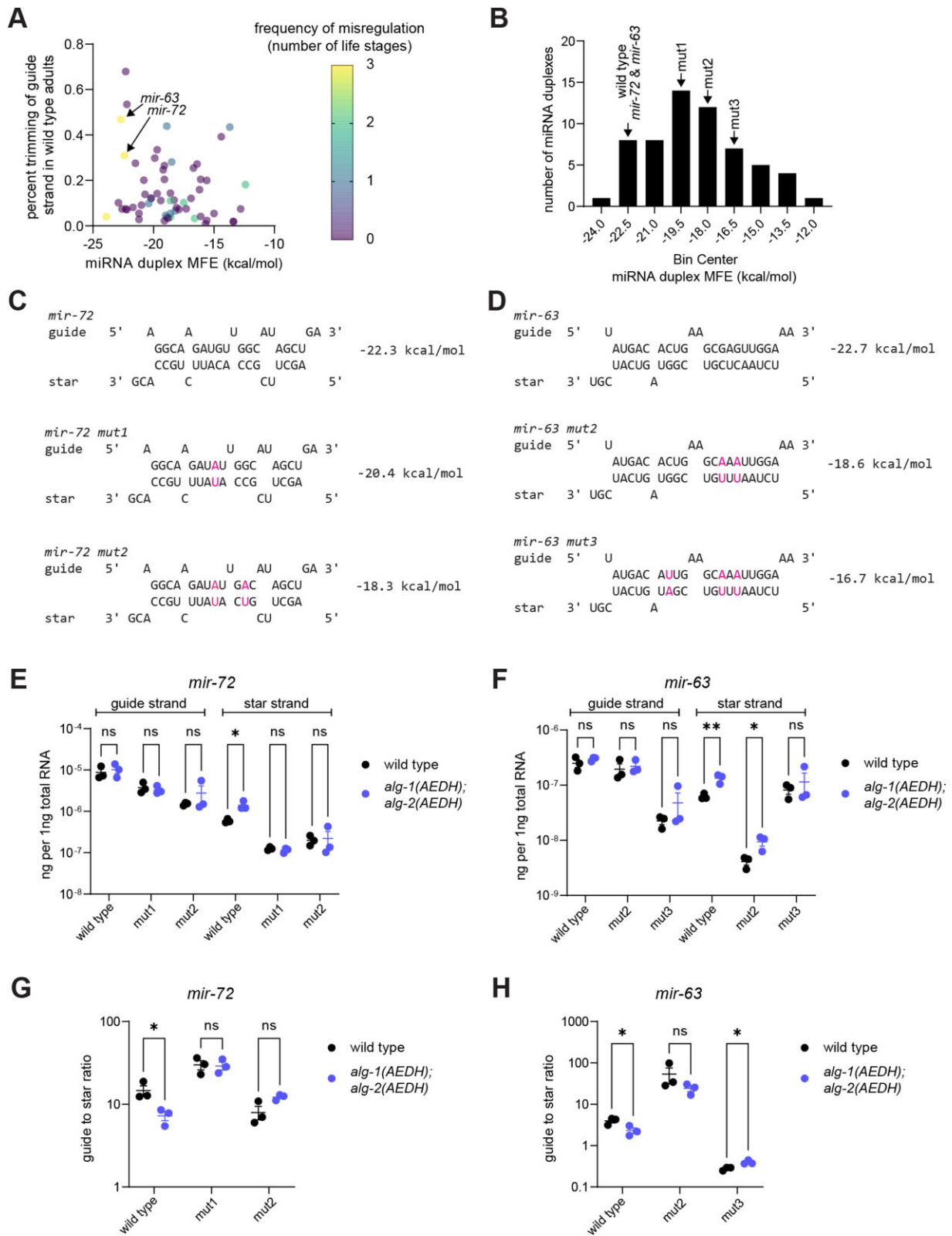


Figure 4. High duplex stability favors a greater role for catalytic residues in unwinding. (A) Percent trimming of guide strand and duplex stability (minimum free energy) of each miRNA duplex. Frequency of star strand misregulation in *alg-1(AEDH)*; *alg-2(AEDH)* among three stages (embryo, L4, adult) is color-coded. (B) Histogram of duplex stabilities with bins containing *mir-63* and *mir-72* and their mutant variants indicated. (A, B) Only miRNAs with sufficient abundance for trimming analysis in (133) are shown. (C, D) Predicted structure of *mir-63* and *mir-72* and engineered mutations in each duplex. (E, F) Absolute quantification by qPCR of *mir-63* and *mir-72* guide and star strands in L4 samples (three biological replicates for each genotype). (G, H) Ratio of guide to star strand calculated from absolute quantification. (E–H) Unpaired *t*-tests, ***P*-value < 0.01, **P*-value < 0.05.

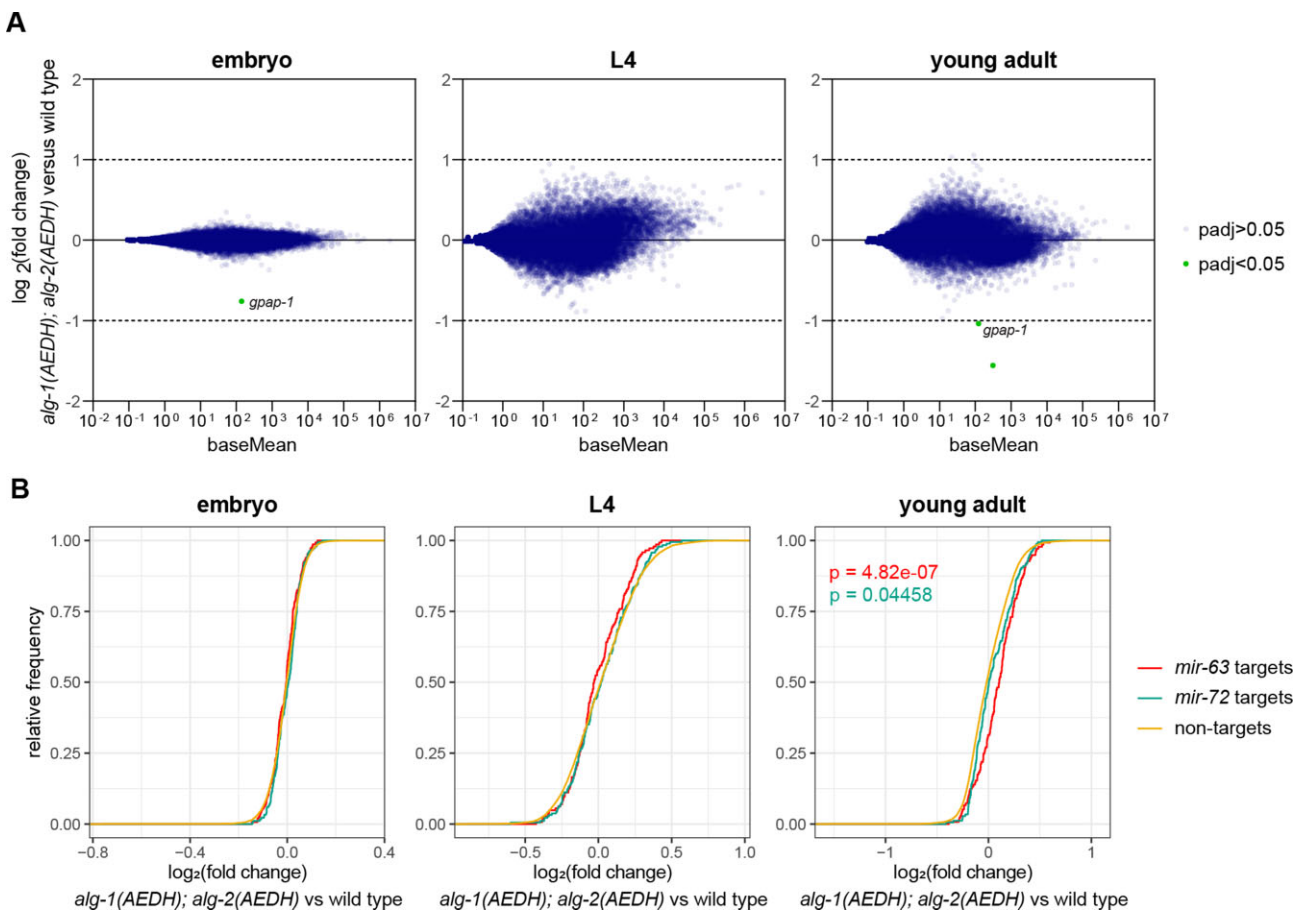


Figure 5. Changes in star strand abundance result in subtle changes in target repression. **(A)** MA plots showing average abundance (of all genes > 10 reads per million) on X-axis and $\log_2(\text{fold change})$ on Y-axis in *alg-1(AEDH); alg-2(AEDH)* versus wild type. Only 1, 0 and 2 genes are significantly altered in expression in embryo, L4 and adult, respectively (DESeq2 $P_{\text{adj}} < 0.05$). **(B)** Empirical cumulative distribution function for $\log_2(\text{fold change})$ values of predicted targets for *mir-63*, *mir-72* or neither (non-targets). Low abundance transcripts (baseMean < 10) were excluded from the analysis. P -values < 0.05 are shown for Kolmogorov-Smirnov test (comparison to non-targets). (A, B) Three (L4) or four (embryo and young adult) biological replicates of each genotype were analyzed.

residues play in miRISC maturation drives only subtle downstream changes in gene expression.

Down-regulation of select guide strands in *alg-1(AEDH); alg-2(AEDH)* mutants is *ebax-1*-independent

In addition to elevation of star strands in the *alg-1(AEDH); alg-2(AEDH)* mutants, decreased levels of a few miRNA guide strands were also observed. The three guide strands that were downregulated in two or more developmental stages were *mir-243-3p*, *mir-1829a-5p*, and *mir-1821-3p*. We sought to formulate a model for why these guides might be downregulated in *alg-1(AEDH); alg-2(AEDH)* based on the features of these miRNAs. *mir-243-3p* was previously shown to be largely loaded into RDE-1 and to act as a siRNA to target a fully complementary site in the 3' UTR of Y47H10A.5 (100). Highly complementary targets can drive target-directed miRNA decay (TDMD); in this process, target cleavage usually does not occur due to a region of central mismatches in the miRNA:target duplex (135,141–153). A minor portion of *mir-243* is bound by ALG-1, and we wondered whether the mild decrease in *mir-243* (as well as *mir-1829a-5p* and *mir-1821-3p*) in *alg-1(AEDH); alg-2(AEDH)* could be due to enhanced

TDMD in the absence of target cleavage (Figure 6A). In this model, TDMD would be less active when ALG-1 is wild type and can cleave the target; when cleavage is inactivated in the *alg-1(AEDH); alg-2(AEDH)* context, TDMD would be more potent, leading to decreased *mir-243* (and other miRNA guide strands) in this mutant (Figure 6A).

We tested this model by inactivating this putative TDMD in two ways: (i) by introducing a null mutation in the TDMD effector EBAX-1 (known as ZSWIM8 in mammals) and (ii) by deleting the binding site for *mir-243* in the Y47H10A.5 3' UTR (100,154–156). If the model is correct, then either of these contexts should abrogate the effect of the *alg-1(AEDH); alg-2(AEDH)* mutations on *mir-243* abundance (Figure 6B). Comparing *ebax-1(null)* young adults to wild type, we corroborate the stabilization of *mir-788*, *mir-247*, *mir-42*, *mir-230*, *mir-797*, *mir-43* and *mir-253* in this mutant as previously observed (Supplementary Figure S7, Supplementary Table S13) (155). (Note that *mir-35-41* are not highly expressed in these samples, which do not contain embryos, in contrast to the previous studies of *ebax-1(null)* which examined gravid adults or embryos (155,157).)

Next, *ebax-1(null)* was introduced to the *alg-1(AEDH); alg-2(AEDH)* background, and miRNA abundances were compared to *ebax-1(null)* single mutants (156). Very sim-

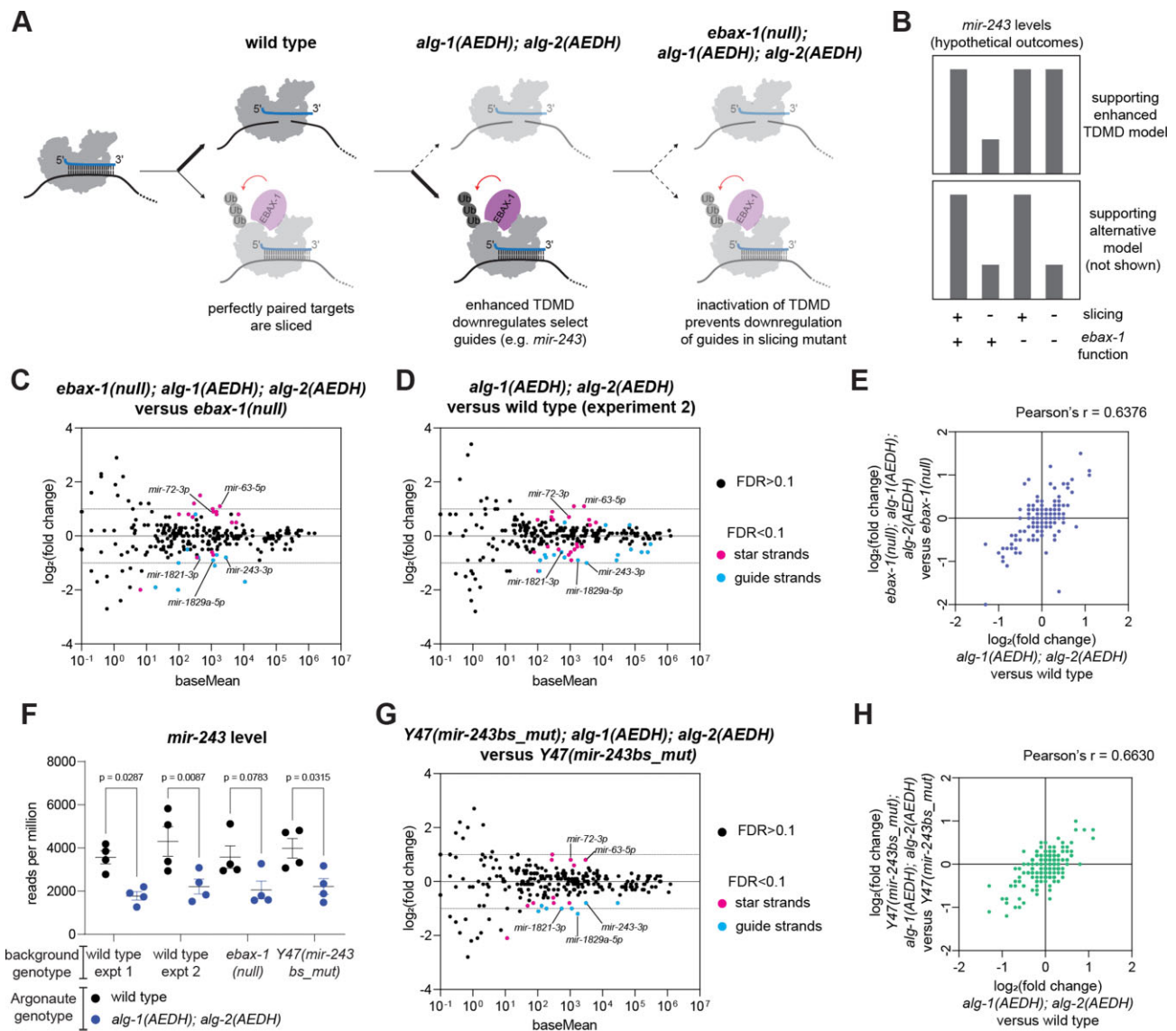


Figure 6. Down-regulation of select guide strands in the catalytic residue mutants is EBAX-1-independent. **(A)** Schematic of model being tested. Highly complementary targets that would otherwise be sliced may instead induce TDMD when slicing is inactivated. **(B)** Possible outcomes that would support the model proposed in **(A)** (top) or support an alternative mechanism (bottom). **(C, D, G)** MA plots showing average abundance on X-axis and $\log_2(\text{fold change})$ on Y-axis. miRNAs showing significant changes are shown in light blue or pink (DESeq2 FDR < 0.1). Genotypes being compared are indicated in graph title. **(E, H)** Correlation of changes induced by *alg-1(AEDH); alg-2(AEDH)* in wild type (X-axis) or *ebax-1(null)* background (Y-axis). **(F)** Level of *mir-243* in each sample after default DESeq2 normalization in pairwise comparisons shown. One-way ANOVA was performed, and *P*-values are from post hoc Sidak's multiple comparisons test. **(E, H)** Only miRNAs with baseMean > 50 in wild type experiment 1 are included. **(C–H)** All samples are young adults. Four biological replicates of each genotype were analyzed.

ilar amplitude in changes were observed when comparing *ebax-1(null); alg-1(AEDH); alg-2(AEDH)* to *ebax-1(null)* (Figure 6C, Supplementary Table S14) as when comparing *alg-1(AEDH); alg-2(AEDH)* to wild type (Figure 6D). The correlation of $\log_2(\text{fold changes})$ across all abundant miRNAs in these two comparisons was fairly strong (Figure 6E, Pearson's $r = 0.6376$) since it was similar to the correlation between two independent experiments of the same genotypes (each experiment including four biological replicates, Supplementary Figure S7B, Supplementary Table S15, Pearson's $r = 0.7173$). This demonstrates that overall the observed effects of *alg-1(AEDH); alg-2(AEDH)* are not EBAX-1-dependent.

When examining the guide strands that were decreased in *alg-1(AEDH); alg-2(AEDH)*, similar downregulation was ob-

served for *mir-243-3p*, *mir-1829a-5p* and *mir-1821-3p* in the *ebax-1(null)* context (Figure 6C, D). Furthermore, the amplitude of downregulation is similar in the *ebax-1(null)* context (Figure 6C–F), and our interpretation is that this downregulation is EBAX-1-independent. Thus, the model that this change is due to enhanced TDMD in the catalytic residue mutant is unsupported by the experiments performed.

The *mir-243* binding site mutant (hereafter *Y47(mir-243bs_del)*) further refuted the model. The decrease of *mir-243* was still observed when comparing *Y47(mir-243bs_del); alg-1(AEDH); alg-2(AEDH)* to *Y47(mir-243bs_del)* single mutants (Figure 6F–H, Supplementary Table S16). This is further evidence negating a role for TDMD in the decrease of select miRNA guide strands in the catalytic residue mutant (also see Discussion).

Discussion

Here, we demonstrate an unexpectedly modest role for catalytic residues in the miRNA pathway in *C. elegans*. Unlike in vertebrates, no miRNA species are strictly dependent upon catalytic residues for their biogenesis or unwinding. Furthermore, target gene expression is only moderately affected as measured by RNAseq. This results in normal development and reproduction in standard laboratory conditions. This work thus overturns the current literature with regard to the importance of miRNA Argonaute catalytic residues in *C. elegans* (13). *C. elegans* is the first animal to our knowledge in which catalytic residues in miRNA Argonautes are conserved but dispensable on an organismal level.

As with any genetic study, some form of compensation could ameliorate phenotypes in animals passaged over multiple generations. The catalytic residue mutations were fairly easy to isolate by CRISPR, and we did not observe stronger phenotypes in early post-CRISPR or post-cross generations, both arguing against strong compensation. Nonetheless, this caveat should be considered, since a compensatory increase in the efficiency of slicing-independent unwinding, for instance, could alleviate the impact of catalytic residue mutations on RISC maturation.

Another caveat to the interpretation of our results is the lack of validation of the impact of the AEDH mutations on slicing via slicing assays. We attempted to perform these assays using recombinant ALG-1/2 produced in insect cells (Sf9 and Hi5) or *E. coli* [BL21 (RIPL)], and we used the AliCE cell-free protein expression system (158). None of these isolates showed efficient slicing by the wild type proteins, although a positive control, human AGO2, did display slicer activity. At this time, we cannot provide a clear explanation for the failure of ALG-1/2 to slice; interpreting this to mean that ALG-1/2 are inherently poor slicers would be premature due to multiple technical hurdles. In all *in vivo* purification systems, the RNA-free fraction of ALG-1/2 was difficult to purify from the RNA-loaded fraction. Yields were very low from the cell-free system, preventing assessment of proper protein folding. Thus, we can neither make assertions about the slicer activity of wild type ALG-1/2 based on these *in vitro* studies, nor assess the impact of the AEDH mutations on slicing. This remains a caveat to our study, despite extensive characterization of the contributions of the residues of the catalytic tetrad to slicing in the context of other Argonaute proteins (159).

Concurrently to this work, the Simard lab also generated and performed molecular and phenotypic analysis of ALG-1 and ALG-2 catalytic residue mutants (Pal *et al.* co-submitted). By examining compound mutants and long-term growth at elevated temperature (25°C), Pal *et al.* observed a greater number of de-regulated miRNAs, though largely overlapping with the changes we observed; prolonged growth at high temperature may contribute to these additional expression changes. Pal *et al.* also observe fitness phenotypes associated with catalytic residue mutations of ALG-1 and/or ALG-2 in the context of prolonged high temperature. Thus, although phenotypes of catalytic residue mutants are much milder than previously thought, they are still apparent in sensitized genetic and physical conditions. These stress-associated phenotypes may provide an experimental framework for understanding the selection pressure for maintaining the catalytic activity of ALG-1 and ALG-2 in the long-term.

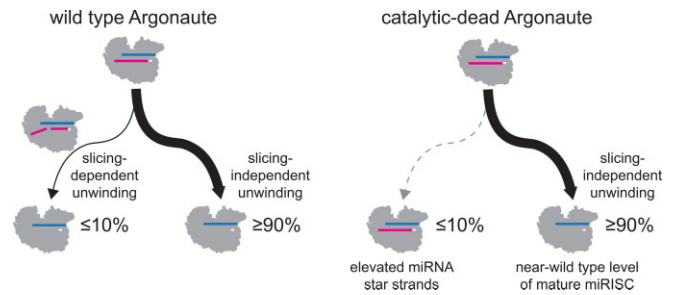


Figure 7. Model of observed effects on miRNA star strands in catalytic residue mutants. A small portion of miRISC maturation depends on catalytic residues. In *alg-1(AEDH);alg-2(AEDH)* mutant backgrounds, this small portion of miRISC retains the star strand (leading to elevated star strand levels). The major portion of miRISC is matured in a slicing-independent manner, thus leaving overall miRISC function largely intact in the mutant background. Dependence of unwinding on catalytic residues is most apparent in embryos in which ALG-2 is highly expressed and for certain thermodynamically-stable miRNA:star duplexes like *mir-63* and *mir-72*. For most miRNAs in L4 and adult samples, dependence of unwinding on catalytic residues is negligible.

Molecularly, the basis of these phenotypes may be related to impaired miRNA:star duplex unwinding. We observed a measurable effect on duplex unwinding, represented by a modest overall stabilization of star strands in embryos (Figure 7). Why is this more prominent in *C. elegans* than other previously studied organisms? By examining single mutant strains, mutant ALG-2 appears to have a greater unwinding defect than mutant ALG-1. ALG-2 may be more dependent upon catalytic residues for unwinding than previously-examined miRNA Argonautes from other organisms. This may be due to either lower efficiency of slicing-independent unwinding or to higher efficiency of slicing of bulged miRNA:star duplexes. Differences in the N terminal domain or non-catalytic residues in the PIWI domain could contribute to either reduced slicing-independent unwinding or enhanced slicing, whereas differences in the PAZ domain could also impair slicing-independent unwinding (17–20,51,80,81,160). This opens up new areas of investigation into the biochemical properties of ALG-2 compared to ALG-1 or Argonautes from other species.

Some miRNA star strands were elevated in catalytic residue mutants in all examined contexts, not only in embryos. The duplexes from which these star strands are derived (*mir-63* and *mir-72*) have fairly high thermodynamic stability. For *mir-72*, we find that this duplex stability is indeed a determinant of its dependence on catalytic residues for unwinding. For *mir-63*, lowering duplex stability did not rescue unwinding in the catalytic residue mutants. Thus, duplex stability is one of the factors that determines the extent of reliance on catalytic residues for unwinding, as previously observed in other settings (48,50,134). However, as illustrated by the case of *mir-63* and the efficient unwinding of even more stable duplexes in catalytic residue mutants (Figure 4A), other uncharacterized factors also control the extent that unwinding depends on catalytic residues. Still, even for *mir-63* and *mir-72*, catalytic residues drive only a minor portion of unwinding; only modest elevation in star strands is observed in catalytic residue mutants, and the vast majority of miRISC matures to the guide-only bound state and properly represses targets (Figure 7).

A more mysterious observation in this study was the decreased levels of a few guide strands. While we explored a model of enhanced TDMD in the catalytic residue mutants, this was not borne out. However, conventional TDMD has yet to be demonstrated in *C. elegans* (133,157,161), so the pathways of slicing and TDMD may not be competing in this context as might be expected in other systems (135,141–155). Because of the modest reduction of these few guide strands, we posit that catalytic residues are not central to their biogenesis. However, slicing could represent one of multiple biogenesis pathways for these guides or somehow regulate their canonical biogenesis. Interestingly, at least two of the three downregulated guides are primarily loaded into an alternative Argonaute: *mir-243-3p* into RDE-1 and *mir-1829a-5p* into ALG-5 (100,129). Could ALG-1/2 cleavage products load into other Argonautes? Precedents for this type of interaction include the loading of Aub and Ago3 cleavage products into each other in the piRNA ping-pong pathway (162). The secondary structures of *mir-243* and *mir-1829a* do not provide a clear parallel, but future experiments may nonetheless reveal some similarity.

Overall, this study of the role of catalytic residues in miRNA Argonautes in a model organism outside the vertebrate lineage showed a surprisingly mild effect on physiology. Although laboratory conditions facilitate the reproducibility to observe clear molecular signatures, they do not recapitulate challenges encountered in the wild. Harsher growth conditions used in a parallel study revealed modest fitness phenotypes associated with catalytic residue mutation (Pal *et al.* co-submitted). The role of catalytic residues in star strand unwinding may suggest a greater role in cold conditions, such as cold shock, where increased duplex stability may disfavor slicing-independent unwinding (50). Robustness of miRISC maturation at a broad range of temperatures may contribute to selection pressure on catalytic residues in the wild. Moreover, our study examined samples derived from whole animals. In the long term, tissue-specific studies may reveal more salient roles for miRISC-mediated slicing not apparent in our study.

Data availability

All deep sequencing raw data can be accessed under SRA Bio-project PRJNA922944.

Supplementary data

Supplementary Data are available at NAR Online.

Acknowledgements

We thank WormBase, the NIDDK Genomics Core, the NCI Genomics Core, and NIH High Performance Computing. Strains are regularly received from and deposited to the CGC, which is funded by NIH Office of Research Infrastructure Programs (P40 OD010440). We thank John Kim for the 3xFLAG::ALG-1 strain (QK67). We thank Amy Pasquinelli and Martin Simard for RNAi clones, and Kevin O'Connell for antibody DM1A. Thank you to Anna Zinovyeva, Martin Simard, and members of the McJunkin lab for helpful discussions.

Funding

NIDDK Intramural Research Program [ZIA DK075147]. Funding for open access charge: NIDDK Intramural Research Program [ZIA DK075147].

Conflict of interest statement

None declared.

References

- Youngman,E.M. and Claycomb,J.M. (2014) From early lessons to new frontiers: the worm as a treasure trove of small RNA biology. *Front. Genet.*, **5**, 416.
- Castel,S.E. and Martienssen,R.A. (2013) RNA interference in the nucleus: roles for small RNAs in transcription, epigenetics and beyond. *Nat. Rev. Genet.*, **14**, 100–112.
- Noto,T. and Mochizuki,K. (2017) Whats, hows and whys of programmed DNA elimination in Tetrahymena. *Open Biol.*, **7**, 170172.
- Tabara,H., Sarkissian,M., Kelly,W.G., Fleenor,J., Grishok,A., Timmons,L., Fire,A. and Mello,C.C. (1999) The rde-1 gene, RNA interference, and transposon silencing in *C. elegans*. *Cell*, **99**, 123–132.
- Grishok,A., Pasquinelli,A.E., Conte,D., Li,N., Parrish,S., Ha,I., Baillie,D.L., Fire,A., Ruvkun,G. and Mello,C.C. (2001) Genes and mechanisms related to RNA interference regulate expression of the small temporal RNAs that control *C. elegans* developmental timing. *Cell*, **106**, 23–34.
- Aoki,K., Moriguchi,H., Yoshioka,T., Okawa,K. and Tabara,H. (2007) In vitro analyses of the production and activity of secondary small interfering RNAs in *C. elegans*. *EMBO J.*, **26**, 5007–5019.
- Liu,J., Carmell,M.A., Rivas,F.V., Marsden,C.G., Thomson,J.M., Song,J.-J., Hammond,S.M., Joshua-Tor,L. and Hannon,G.J. (2004) Argonaute2 is the catalytic engine of mammalian RNAi. *Science*, **305**, 1437–1441.
- Song,J.-J., Smith,S.K., Hannon,G.J. and Joshua-Tor,L. (2004) Crystal structure of Argonaute and its implications for RISC slicer activity. *Science*, **305**, 1434–1437.
- Rivas,F.V., Tolia,N.H., Song,J.J., Aragon,J.P., Liu,J., Hannon,G.J. and Joshua-Tor,L. (2005) Purified Argonaute2 and an siRNA form recombinant human RISC. *Nat. Struct. Mol. Biol.*, **12**, 340–349.
- Rand,T.A., Ginalski,K., Grishin,N.V. and Wang,X. (2004) Biochemical identification of Argonaute 2 as the sole protein required for RNA-induced silencing complex activity. *Proc. Natl. Acad. Sci. U.S.A.*, **101**, 14385–14389.
- Meister,G., Landthaler,M., Patkaniowska,A., Dorsett,Y., Teng,G. and Tuschl,T. (2004) Human Argonaute2 mediates RNA cleavage targeted by miRNAs and siRNAs. *Mol. Cell*, **15**, 185–197.
- Steiner,F.A., Okihara,K.L., Hoogstrate,S.W., Sijen,T. and Ketting,R.F. (2009) RDE-1 slicer activity is required only for passenger-strand cleavage during RNAi in *Caenorhabditis elegans*. *Nat. Struct. Mol. Biol.*, **16**, 207–211.
- Bouasker,S. and Simard,M.J. (2012) The slicing activity of miRNA-specific argonautes is essential for the miRNA pathway in *C. elegans*. *Nucleic Acids Res.*, **40**, 10452–10462.
- Yigit,E., Batista,P.J., Bei,Y., Pang,K.M., Chen,C.C.G., Tolia,N.H., Joshua-Tor,L., Mitani,S., Simard,M.J. and Mello,C.C. (2006) Analysis of the *C. elegans* Argonaute family reveals that distinct Argonautes act sequentially during RNAi. *Cell*, **127**, 747–757.
- Nakanishi,K., Weinberg,D.E., Bartel,D.P. and Patel,D.J. (2012) Structure of yeast argonaute with guide RNA. *Nature*, **486**, 368–374.
- Yuan,Y.R., Pei,Y., Ma,J.B., Kuryavyi,V., Zhadina,M., Meister,G., Chen,H.Y., Dauter,Z., Tuschl,T. and Patel,D.J. (2005) Crystal structure of *A. aeolicus* argonaute, a site-specific DNA-guided

- endoribonuclease, provides insights into RISC-mediated mRNA cleavage. *Mol. Cell*, **19**, 405–419.
17. Faehnle, C.R., Elkayam, E., Haase, A.D., Hannon, G.J. and Joshua-Tor, L. (2013) The making of a slicer: activation of Human Argonaute-1. *Cell Rep.*, **3**, 1901–1909.
 18. Hauptmann, J., Dueck, A., Harlander, S., Pfaff, J., Merkl, R. and Meister, G. (2013) Turning catalytically inactive human Argonaute proteins into active slicer enzymes. *Nat. Struct. Mol. Biol.*, **20**, 814–817.
 19. Hauptmann, J., Kater, L., Löffler, P., Merkl, R. and Meister, G. (2014) Generation of catalytic human Ago4 identifies structural elements important for RNA cleavage. *RNA*, **20**, 1532–1538.
 20. Schürmann, N., Trabuco, L.G., Bender, C., Russell, R.B. and Grimm, D. (2013) Molecular dissection of human Argonaute proteins by DNA shuffling. *Nat. Struct. Mol. Biol.*, **20**, 818–826.
 21. Nakanishi, K., Ascano, M., Gogakov, T., Ishibe-Murakami, S., Serganov, A.A., Briskin, D., Morozov, P., Tuschl, T. and Patel, D.J. (2013) Eukaryote-specific insertion elements control Human ARGONAUTE slicer activity. *Cell Rep.*, **3**, 1893–1900.
 22. Brennecke, J., Aravin, A.A., Stark, A., Dus, M., Kellis, M., Sachidanandam, R. and Hannon, G.J. (2007) Discrete small RNA-generating loci as master regulators of transposon activity in *Drosophila*. *Cell*, **128**, 1089–1103.
 23. Gunawardane, L.S., Saito, K., Nishida, K.M., Miyoshi, K., Kawamura, Y., Nagami, T., Siomi, H. and Siomi, M.C. (2007) A slicer-mediated mechanism for repeat-associated siRNA 5' end formation in *Drosophila*. *Science*, **315**, 1587–1590.
 24. Aravin, A.A., Sachidanandam, R., Girard, A., Fejes-Toth, K. and Hannon, G.J. (2007) Developmentally regulated piRNA clusters implicate MILI in transposon control. *Science*, **316**, 744–747.
 25. De Fazio, S., Bartonicek, N., Di Giacomo, M., Abreu-Goodger, C., Sankar, A., Funaya, C., Antony, C., Moreira, P.N., Enright, A.J. and O'carroll, D. (2011) The endonuclease activity of Mili fuels piRNA amplification that silences LINE1 elements. *Nature*, **480**, 259–263.
 26. Perez-Borrajero, C., Podvalnaya, N., Holleis, K., Lichtenberger, R., Karaulanov, E., Simon, B., Basquin, J., Hennig, J., Ketting, R.F. and Falk, S. (2021) Structural basis of PETISCO complex assembly during piRNA biogenesis in *C. elegans*. *Genes Dev.*, **35**, 1304–1323.
 27. Podvalnaya, N., Bronkhorst, A.W., Lichtenberger, R., Hellmann, S., Nischwitz, E., Falk, T., Karaulanov, E., Butter, F., Falk, S. and Ketting, R.F. (2023) piRNA processing by a trimeric Schlafen-domain nuclease. *Nature*, **622**, 402–409.
 28. Ruby, J.G., Jan, C., Player, C., Axtell, M.J., Lee, W., Nusbaum, C., Ge, H. and Bartel, D.P. (2006) Large-scale sequencing reveals 21U-RNAs and additional microRNAs and endogenous siRNAs in *C. elegans*. *Cell*, **127**, 1193–1207.
 29. Gu, W., Lee, H.C., Chaves, D., Youngman, E.M., Pazour, G.J., Conte, D. and Mello, C.C. (2012) CapSeq and CIP-TAP identify Pol II start sites and reveal capped small RNAs as *C. elegans* piRNA precursors. *Cell*, **151**, 1488–1500.
 30. Fromm, B., Billipp, T., Peck, L.E., Johansen, M., Tarver, J.E., King, B.L., Newcomb, J.M., Sempere, L.F., Flatmark, K., Hovig, E., et al. (2015) A Uniform System for the Annotation of Vertebrate microRNA Genes and the Evolution of the Human microRNAome. *Annu. Rev. Genet.*, **49**, 213–242.
 31. Billi, A.C., Freeberg, M.A., Day, A.M., Chun, S.Y., Khivansara, V. and Kim, J.K. (2013) A conserved upstream motif orchestrates autonomous, germline-enriched expression of *Caenorhabditis elegans* piRNAs. *PLoS Genet.*, **9**, e1003392.
 32. Das, P.P., Bagijn, M.P., Goldstein, L.D., Woolford, J.R., Lehrbach, N.J., Sapetschnig, A., Buhecha, H.R., Gilchrist, M.J., Howe, K.L., Stark, R., et al. (2008) Piwi and piRNAs act upstream of an endogenous siRNA pathway to suppress Tc3 transposon mobility in the *Caenorhabditis elegans* germline. *Mol. Cell*, **31**, 79–90.
 33. Zeng, C., Weng, C., Wang, X., Yan, Y.H., Li, W.J., Xu, D., Hong, M., Liao, S., Dong, M.Q., Feng, X., et al. (2019) Functional proteomics identifies a PICS complex required for piRNA maturation and chromosome segregation. *Cell Rep.*, **27**, 3561–3572.
 34. Wang, X., Zeng, C., Liao, S., Zhu, Z., Zhang, J., Tu, X., Yao, X., Feng, X., Guang, S. and Xu, C. (2021) Molecular basis for PICS-mediated piRNA biogenesis and cell division. *Nat. Commun.*, **12**, 5595.
 35. Weick, E.M., Sarkies, P., Silva, N., Chen, R.A., Moss, S.M.M., Cording, A.C., Ahringer, J., Martinez-Perez, E. and Miska, E.A. (2014) PRDE-1 is a nuclear factor essential for the biogenesis of Ruby motif-dependent piRNAs in *C. elegans*. *Genes Dev.*, **28**, 783–796.
 36. Cordeiro Rodrigues, R.J., De Jesus Domingues, A.M., Hellmann, S., Dietz, S., De Albuquerque, B.F.M., Renz, C., Ulrich, H.D., Sarkies, P., Butter, F. and Ketting, R.F. (2019) PETISCO is a novel protein complex required for 21U RNA biogenesis and embryonic viability. *Genes Dev.*, **33**, 857–870.
 37. Goh, W.S.S., Seah, J.W.E., Harrison, E.J., Chen, C., Hammell, C.M. and Hannon, G.J. (2014) A genome-wide RNAi screen identifies factors required for distinct stages of *C. elegans* piRNA biogenesis. *Genes Dev.*, **28**, 797–807.
 38. Pastore, B., Hertz, H.L., Price, I.F. and Tang, W. (2021) pre-piRNA trimming and 2'-O-methylation protect piRNAs from 3' tailing and degradation in *C. elegans*. *Cell Rep.*, **36**, 109640.
 39. Montgomery, T.A., Rim, Y.S., Zhang, C., Dowen, R.H., Phillips, C.M., Fischer, S.E.J. and Ruvkun, G. (2012) PIWI associated siRNAs and piRNAs specifically require the *Caenorhabditis elegans* HEN1 ortholog henn-1. *PLoS Genet.*, **8**, e1002616.
 40. Billi, A.C., Alessi, A.F., Khivansara, V., Han, T., Freeberg, M., Mitani, S. and Kim, J.K. (2012) The *Caenorhabditis elegans* HEN1 ortholog, HENN-1, methylates and stabilizes select subclasses of germline small RNAs. *PLoS Genet.*, **8**, e1002617.
 41. Kamminga, L.M., van Wolfswinkel, J.C., Luteijn, M.J., Kaaij, L.J.T., Bagijn, M.P., Sapetschnig, A., Miska, E.A., Berezikov, E. and Ketting, R.F. (2012) Differential impact of the HEN1 homolog HENN-1 on 21U and 26G RNAs in the germline of *Caenorhabditis elegans*. *PLoS Genet.*, **8**, e1002702.
 42. Tang, W., Tu, S., Lee, H.C., Weng, Z. and Mello, C.C. (2016) The RNase PARN-1 trims piRNA 3' ends to promote transcriptome surveillance in *C. elegans*. *Cell*, **164**, 974–984.
 43. Singh, M., Cornes, E., Li, B., Quarato, P., Bourdon, L., Dingli, F., Loew, D., Proccaccia, S. and Cecere, G. (2021) Translation and codon usage regulate argonaute slicer activity to trigger small RNA biogenesis. *Nat Commun.*, **12**, 3492.
 44. Matranga, C., Tomari, Y., Shin, C., Bartel, D.P. and Zamore, P.D. (2005) Passenger-strand cleavage facilitates assembly of siRNA into Ago2-containing RNAi enzyme complexes. *Cell*, **123**, 607–620.
 45. Miyoshi, K., Tsukumo, H., Nagami, T., Siomi, H. and Siomi, M.C. (2005) Slicer function of *Drosophila* Argonautes and its involvement in RISC formation. *Genes Dev.*, **19**, 2837–2848.
 46. Leuschner, P.J.F., Ameres, S.L., Kueng, S. and Martinez, J. (2006) Cleavage of the siRNA passenger strand during RISC assembly in human cells. *EMBO Rep.*, **7**, 314–320.
 47. Rand, T.A., Petersen, S., Du, F. and Wang, X. (2005) Argonaute2 cleaves the anti-guide strand of siRNA during RISC activation. *Cell*, **123**, 621–629.
 48. Kawamata, T., Seitz, H. and Tomari, Y. (2009) Structural determinants of miRNAs for RISC loading and slicer-independent unwinding. *Nat. Struct. Mol. Biol.*, **16**, 953–960.
 49. Shin, C. (2008) Cleavage of the star strand facilitates assembly of some MicroRNAs into Ago2-containing silencing complexes in mammals. *Mol. Cells*, **26**, 308–313.
 50. Park, J.H. and Shin, C. (2015) Slicer-independent mechanism drives small-RNA strand separation during human RISC assembly. *Nucleic Acids Res.*, **43**, 9418–9433.
 51. Kwak, P.B. and Tomari, Y. (2012) The N domain of Argonaute drives duplex unwinding during RISC assembly. *Nat. Struct. Mol. Biol.*, **19**, 145–151.

52. Wu, P.H., Fu, Y., Cecchini, K., Özata, D.M., Arif, A., Yu, T., Colpan, C., Gainetdinov, I., Weng, Z. and Zamore, P.D. (2020) The evolutionarily conserved piRNA-producing locus pi6 is required for male mouse fertility. *Nat. Genet.*, **52**, 728–739.
53. Goh, W.S.S., Falcatori, I., Tam, O.H., Burgess, R., Meikar, O., Kotaja, N., Hammell, M. and Hannon, G.J. (2015) piRNA-directed cleavage of meiotic transcripts regulates spermatogenesis. *Genes Dev.*, **29**, 1032–1044.
54. Vourekas, A., Zheng, Q., Alexiou, P., Maragkakis, M., Kirino, Y., Gregory, B.D. and Mourelatos, Z. (2012) Mili and Miwi target RNA repertoire reveals piRNA biogenesis and function of Miwi in spermiogenesis. *Nat. Struct. Mol. Biol.*, **19**, 773–781.
55. Zhang, P., Kang, J.Y., Gou, L.T., Wang, J., Xue, Y., Skogerboe, G., Dai, P., Huang, D.W., Chen, R., Fu, X.D., *et al.* (2015) MIWI and piRNA-mediated cleavage of messenger RNAs in mouse testes. *Cell Res.*, **25**, 193–207.
56. Reuter, M., Berninger, P., Chuma, S., Shah, H., Hosokawa, M., Funaya, C., Antony, C., Sachidanandam, R. and Pillai, R.S. (2011) Miwi catalysis is required for piRNA amplification-independent LINE1 transposon silencing. *Nature*, **480**, 264–267.
57. Bagijn, M.P., Goldstein, L.D., Sapetschnig, A., Weick, E.M., Bouasker, S., Lehrbach, N.J., Simard, M.J. and Miska, E.A. (2012) Function, targets, and evolution of *Caenorhabditis elegans* piRNAs. *Science*, **337**, 574–578.
58. Shirayama, M., Seth, M., Lee, H.-C., Gu, W., Ishidate, T., Conte, D. J. and Mello, C.C. (2012) piRNAs initiate an epigenetic memory of nonself RNA in the *C. elegans* germline. *Cell*, **150**, 65–77.
59. Lee, H.C., Gu, W., Shirayama, M., Youngman, E., Conte, D. and Mello, C.C. (2012) *C. elegans* piRNAs mediate the genome-wide surveillance of germline transcripts. *Cell*, **150**, 78–87.
60. Ashe, A., Sapetschnig, A., Weick, E.M., Mitchell, J., Bagijn, M.P., Cording, A.C., Doebley, A.L., Goldstein, L.D., Lehrbach, N.J., Le Pen, J., *et al.* (2012) piRNAs can trigger a multigenerational epigenetic memory in the germline of *C. elegans*. *Cell*, **150**, 88–99.
61. Gerson-Gurwitz, A., Wang, S., Sathe, S., Green, R., Yeo, G.W., Oegema, K. and Desai, A. (2016) A small RNA-catalytic argonaute pathway tunes germline transcript levels to ensure embryonic divisions. *Cell*, **165**, 396–409.
62. Quarato, P., Singh, M., Cornes, E., Li, B., Bourdon, L., Mueller, F., Didier, C. and Cecere, G. (2021) Germline inherited small RNAs facilitate the clearance of untranslated maternal mRNAs in *C. elegans* embryos. *Nat. Commun.*, **12**, 1441.
63. Avgousti, D.C., Palani, S., Sherman, Y. and Grishok, A. (2012) CSR-1 RNAi pathway positively regulates histone expression in *C. elegans*. *EMBO J.*, **31**, 3821–3832.
64. van Wolfswinkel, J.C., Claycomb, J.M., Batista, P.J., Mello, C.C., Berezikov, E. and Ketting, R.F. (2009) CDE-1 affects chromosome segregation through uridylation of CSR-1-bound siRNAs. *Cell*, **139**, 135–148.
65. Claycomb, J.M., Batista, P.J., Pang, K.M., Gu, W., Vasale, J.J., van Wolfswinkel, J.C., Chaves, D.A., Shirayama, M., Mitani, S., Ketting, R.F., *et al.* (2009) The Argonaute CSR-1 and its 22G-RNA cofactors are required for holocentric chromosome segregation. *Cell*, **139**, 123–134.
66. Wedeles, C.J., Wu, M.Z. and Claycomb, J.M. (2013) Protection of germline gene expression by the *C. elegans* Argonaute CSR-1. *Dev. Cell*, **27**, 664–671.
67. Seth, M., Shirayama, M., Gu, W., Ishidate, T., Conte, D. and Mello, C.C. (2013) The *C. elegans* CSR-1 argonaute pathway counteracts epigenetic silencing to promote germline gene expression. *Dev. Cell*, **27**, 656–663.
68. Cecere, G., Hoersch, S., O'keeffe, S., Sachidanandam, R. and Grishok, A. (2014) Global effects of the CSR-1 RNA interference pathway on the transcriptional landscape. *Nat. Struct. Mol. Biol.*, **21**, 358–365.
69. Park, M.S., Sim, G.Y., Kehling, A.C. and Nakanishi, K. (2020) Human Argonaute2 and Argonaute3 are catalytically activated by different lengths of guide RNA. *Proc. Natl. Acad. Sci. U.S.A.*, **117**, 28576–28578.
70. Nakanishi, K. (2022) Anatomy of four human Argonaute proteins. *Nucleic Acids Res.*, **50**, 6618–6638.
71. Arif, A., Bailey, S., Izumi, N., Anzelon, T.A., Ozata, D.M., Andersson, C., Gainetdinov, I., MacRae, I.J., Tomari, Y. and Zamore, P.D. (2022) GTSF1 accelerates target RNA cleavage by PIWI-clade Argonaute proteins. *Nature*, **608**, 618–625.
72. Park, M.S., Phan, H.D., Busch, F., Hinckley, S.H., Brackbill, J.A., Wysocki, V.H. and Nakanishi, K. (2017) Human Argonaute3 has slicer activity. *Nucleic Acids Res.*, **45**, 11867–11877.
73. Wang, P.Y. and Bartel, D.P. (2023) The guide RNA sequence dictates the slicing kinetics and conformational dynamics of the Argonaute silencing complex. bioRxiv doi: <https://doi.org/10.1101/2023.10.15.562437>, 16 October 2023, preprint: not peer reviewed.
74. Bernstein, E., Caudy, A.A., Hammond, S.M. and Hannon, G.J. (2001) Role for a bidentate ribonuclease in the initiation step of RNA interference. *Nature*, **409**, 363–366.
75. Ketting, R.F., Fischer, S.E., Bernstein, E., Sijen, T., Hannon, G.J. and Plasterk, R.H. (2001) Dicer functions in RNA interference and in synthesis of small RNA involved in developmental timing in *C. elegans*. *Genes Dev.*, **15**, 2654–2659.
76. Knight, S.W. and Bass, B.L. (2001) A role for the RNase III enzyme DCR-1 in RNA interference and germ line development in *Caenorhabditis elegans*. *Science*, **293**, 2269–2271.
77. Cheloufi, S., Dos Santos, C.O., Chong, M.M.W. and Hannon, G.J. (2010) A dicer-independent miRNA biogenesis pathway that requires ago catalysis. *Nature*, **465**, 584–589.
78. Cifuentes, D., Xue, H., Taylor, D.W., Patnode, H., Mishima, Y.Y., Cheloufi, S., Ma, E., Mane, S., Hannon, G.J., Lawson, N.D., *et al.* (2010) A novel miRNA processing pathway independent of Dicer requires Argonaute2 catalytic activity. *Science*, **328**, 1694–1698.
79. Yang, S., Maurin, T., Robine, N., Rasmussen, K.D., Jeffrey, K.L., Chandwani, R., Papapetrou, E.P., Sadelain, M., O'Carroll, D. and Lai, E.C. (2010) Conserved vertebrate mir-451 provides a platform for dicer-independent, Ago2-mediated microRNA biogenesis. *Proc. Natl. Acad. Sci. USA*, **107**, 15163–15168.
80. Zinovyeva, A.Y., Bouasker, S., Simard, M.J., Hammell, C.M. and Ambros, V. (2014) Mutations in conserved residues of the *C. elegans* microRNA argonaute ALG-1 identify separable functions in ALG-1 miRISC loading and target repression. *PLoS Genet.*, **10**, e1004286.
81. Zinovyeva, A.Y., Veksler-Lublinsky, I., Vashisht, A.A., Wohlschlegel, J.A., Ambros, V.R. and Horvitz, H.R. (2015) *Caenorhabditis elegans* ALG-1 antimorphic mutations uncover functions for argonaute in microRNA guide strand selection and passenger strand disposal. *Proc. Natl. Acad. Sci. U.S.A.*, **112**, E5271–E5280.
82. Jee, D., Yang, J.S., Park, S.M., Farmer, D.T., Wen, J., Chou, T., Chow, A., McManus, M.T., Kharas, M.G. and Lai, E.C. (2018) Dual strategies for Argonaute2-mediated biogenesis of erythroid miRNAs underlie conserved requirements for slicing in mammals. *Mol. Cell*, **69**, 265–278.
83. Fromm, B., Billipp, T., Peck, L.E., Johansen, M., Tarver, J.E., King, B.L., Newcomb, J.M., Sempere, L.F., Flatmark, K., Hovig, E., *et al.* (2015) A uniform system for the annotation of vertebrate microRNA genes and the evolution of the Human microRNAome. **49**, 213–242.
84. Lee, R.C., Feinbaum, R.L. and Ambros, V. (1993) The *C. elegans* heterochronic gene *lin-4* encodes small RNAs with antisense complementarity to *lin-14*. *Cell*, **75**, 843–854.
85. Wightman, B., Ha, J. and Ruvkun, G. (1993) Posttranscriptional regulation of the heterochronic gene *lin-14* by *lin-4* mediates temporal pattern formation in *C. elegans*. *Cell*, **75**, 855–862.
86. Ha, J., Wightman, B. and Ruvkun, G. (1996) A bulged *lin-4*/*lin-14* RNA duplex is sufficient for *Caenorhabditis elegans* *lin-14* temporal gradient formation. *Genes Dev.*, **10**, 3041–3050.

87. Vella, M.C., Choi, E.Y., Lin, S.Y., Reinert, K. and Slack, F.J. (2004) The *C. elegans* microRNA let-7 binds to imperfect let-7 complementary sites from the lin-41 3'UTR. *Genes Dev.*, **18**, 132–137.
88. Bagga, S., Bracht, J., Hunter, S., Massirer, K., Holtz, J., Eachus, R. and Pasquinelli, A.E. (2005) Regulation by let-7 and lin-4 miRNAs results in target mRNA degradation. *Cell*, **122**, 553–563.
89. Olsen, P.H. and Ambros, V. (1999) The lin-4 regulatory RNA controls developmental timing in *Caenorhabditis elegans* by blocking LIN-14 protein synthesis after the initiation of translation. *Dev. Biol.*, **216**, 671–680.
90. Seggerson, K., Tang, L. and Moss, E.G. (2002) Two genetic circuits repress the *Caenorhabditis elegans* heterochronic gene lin-28 after translation initiation. *Dev. Biol.*, **243**, 215–225.
91. Wu, E., Thivierge, C., Flamand, M., Mathonnet, G., Vashisht, A.A., Wohlschlegel, J., Fabian, M.R., Sonenberg, N. and Duchaine, T.F. (2010) Pervasive and cooperative deadenylation of 3'UTRs by embryonic microRNA families. *Mol. Cell*, **40**, 558–570.
92. Dallaire, A., Frédérick, P.-M.M. and Simard, M.J. (2018) Somatic and germline MicroRNAs form distinct silencing complexes to regulate their target mRNAs differently. *Dev. Cell*, **47**, 239–247.
93. Mayya, V.K., Flamand, M.N., Lambert, A.M., Jafarnejad, S.M., Wohlschlegel, J.A., Sonenberg, N. and Duchaine, T.F. (2021) MicroRNA-mediated translation repression through GYF-1 and IFE-4 in *C. elegans* development. *Nucleic Acids Res.*, **49**, 4803–4815.
94. Yekta, S., Shih, I.-H.H. and Bartel, D.P. (2004) MicroRNA-directed cleavage of HOXB8 mRNA. *Science*, **304**, 594–596.
95. Ding, L., Spencer, A., Morita, K. and Han, M. (2005) The developmental timing regulator AIN-1 interacts with miRISCs and may target the argonaute protein ALG-1 to cytoplasmic P bodies in *C. elegans*. *Mol. Cell*, **19**, 437–447.
96. Jannot, G., Michaud, P., Quévillon Huberdeau, M., Morel-Berryman, L., Brackbill, J.A., Piquet, S., McJunkin, K., Nakanishi, K. and Simard, M.J. (2016) GW182-Free microRNA silencing complex controls post-transcriptional gene expression during *Caenorhabditis elegans* embryogenesis. *PLoS Genet.*, **12**, e1006484.
97. Davis, E., Caiment, F., Tordoir, X., Cavallé, J., Ferguson-Smith, A., Cockett, N., Georges, M. and Charlier, C. (2005) RNAi-mediated allelic trans-interaction at the imprinted Rtl1/Peg11 locus. *Curr. Biol.*, **15**, 743–749.
98. Karginov, F.V., Cheloufi, S., Chong, M.M.W., Stark, A., Smith, A.D. and Hannon, G.J. (2010) Diverse endonucleolytic cleavage sites in the mammalian transcriptome depend upon microRNAs, Drosha, and additional nucleases. *Mol. Cell*, **38**, 781–788.
99. Shin, C., Nam, J.W., Farh, K.K.H., Chiang, H.R., Shkumatava, A. and Bartel, D.P. (2010) Expanding the microRNA targeting code: functional sites with centered pairing. *Mol. Cell*, **38**, 789–802.
100. Corrêa, R.L., Steiner, F.A., Berezikov, E. and Ketting, R.F. (2010) MicroRNA-directed siRNA biogenesis in *Caenorhabditis elegans*. *PLoS Genet.*, **6**, e1000903.
101. Bracken, C.P., Szubert, J.M., Mercer, T.R., Dinger, M.E., Thomson, D.W., Mattick, J.S., Michael, M.Z. and Goodall, G.J. (2011) Global analysis of the mammalian RNA degradome reveals widespread miRNA-dependent and miRNA-independent endonucleolytic cleavage. *Nucleic Acids Res.*, **39**, 5658–5668.
102. Park, J.H., Ahn, S., Kim, S., Lee, J., Nam, J.W. and Shin, C. (2013) Degradome sequencing reveals an endogenous microRNA target in *C. elegans*. *FEBS Lett.*, **587**, 964–969.
103. Moran, Y., Fredman, D., Praher, D., Li, X.Z., Wee, L.M., Rentzsch, F., Zamore, P.D., Technau, U. and Seitz, H. (2014) Cnidarian microRNAs frequently regulate targets by cleavage. *Genome Res.*, **24**, 651.
104. Inukai, S., Pincus, Z., De Lencastre, A. and Slack, F.J. (2018) A microRNA feedback loop regulates global microRNA abundance during aging. *RNA*, **24**, 159–172.
105. Stein, P., Rozhkov, N.V., Li, F., Cárdenas, F.L., Davydenko, O., Vandivier, L.E., Gregory, B.D., Hannon, G.J. and Schultz, R.M. (2015) Essential role for endogenous siRNAs during meiosis in mouse oocytes. *PLoS Genet.*, **11**, e1005013.
106. Batista, P.J., Ruby, J.G., Claycomb, J.M., Chiang, R., Fahlgren, N., Kasschau, K.D., Chaves, D.A., Gu, W., Vasale, J.J., Duan, S., et al. (2008) PRG-1 and 21U-RNAs interact to form the piRNA complex required for fertility in *C. elegans*. *Mol. Cell*, **31**, 67–78.
107. Seroussi, U., Lugowski, A., Wadi, L., Lao, R.X., Willis, A.R., Zhao, W., Sundby, A.E., Charlesworth, A.G., Reinke, A.W. and Claycomb, J.M. (2023) A comprehensive survey of *C. elegans* argonaute proteins reveals organism-wide gene regulatory networks and functions. *eLife*, **12**, e83853.
108. Conine, C.C., Moresco, J.J., Gu, W., Shirayama, M., Conte, D. Jr, Yates, J.R. 3rd and Mello, C.C. (2013) Argonautes promote male fertility and provide a paternal memory of germline gene expression in *C. elegans*. *Cell*, **155**, 1532–1544.
109. Conine, C.C., Batista, P.J., Gu, W., Claycomb, J.M., Chaves, D.A., Shirayama, M. and Mello, C.C. (2010) Argonautes ALG-3 and ALG-4 are required for spermatogenesis-specific 26G-RNAs and thermotolerant sperm in *Caenorhabditis elegans*. *Proc. Natl. Acad. Sci. U.S.A.*, **107**, 3588–3593.
110. Gent, J.I., Lamm, A.T., Pavelec, D.M., Maniar, J.M., Parameswaran, P., Tao, L., Kennedy, S. and Fire, A.Z. (2010) Distinct phases of siRNA synthesis in an endogenous RNAi pathway in *C. elegans* soma. *Mol. Cell*, **37**, 679–689.
111. Gu, W., Shirayama, M., Conte, D., Vasale, J., Batista, P.J., Claycomb, J.M., Moresco, J.J., Youngman, E.M., Keys, J., Stoltz, M.J., et al. (2009) Distinct argonaute-mediated 22G-RNA pathways direct genome surveillance in the *C. elegans* germline. *Mol. Cell*, **36**, 231–244.
112. Guang, S., Bochner, A.F., Pavelec, D.M., Burkhart, K.B., Harding, S., Lachowicz, J. and Kennedy, S. (2008) An Argonaute transports siRNAs from the cytoplasm to the nucleus. *Science*, **321**, 537–541.
113. Buckley, B.A., Burkhart, K.B., Gu, S.G., Spracklin, G., Kershner, A., Fritz, H., Kimble, J., Fire, A. and Kennedy, S. (2012) A nuclear Argonaute promotes multigenerational epigenetic inheritance and germline immortality. *Nature*, **489**, 447–451.
114. Steiner, F.A., Hoogstrate, S.W., Okihara, K.L., Thijssen, K.L., Ketting, R.F., Plasterk, R.H.A. and Sijen, T. (2007) Structural features of small RNA precursors determine Argonaute loading in *Caenorhabditis elegans*. *Nat. Struct. Mol. Biol.*, **14**, 927–933.
115. Stiernagle, T. (2006) Maintenance of *C. elegans*. In: *WormBook: The Online Review of C. elegans Biology*. Pasadena (CA), <https://doi.org/10.1895/wormbook.1.101.1>.
116. Yang, B., Schwartz, M. and McJunkin, K. (2020) In vivo CRISPR screening for phenotypic targets of the mir-35-42 family in *C. elegans*. *Genes Dev.*, **34**, 1227–1238.
117. Moreno-Mateos, M.A., Vejnar, C.E., Beaudoin, J.D., Fernandez, J.P., Mis, E.K., Khokha, M.K. and Giraldez, A.J. (2015) CRISPRscan: designing highly efficient sgRNAs for CRISPR-Cas9 targeting in vivo. *Nat. Methods*, **12**, 982–988.
118. Paix, A., Wang, Y., Smith, H.E., Lee, C.Y.S., Calidas, D., Lu, T., Smith, J., Schmidt, H., Krause, M.W. and Seydoux, G. (2014) Scalable and versatile genome editing using linear DNAs with microhomology to Cas9 sites in *Caenorhabditis elegans*. *Genetics*, **198**, 1347–1356.
119. Arribere, J.A., Bell, R.T., Fu, B.X.H., Artiles, K.L., Hartman, P.S. and Fire, A.Z. (2014) Efficient marker-free recovery of custom genetic modifications with CRISPR/Cas9 in *Caenorhabditis elegans*. *Genetics*, **198**, 837–846.
120. Duan, Y., Choi, S., Nelson, C. and Ambros, V. (2020) Engineering essential genes with a 'jump board' strategy using CRISPR/Cas9. *Micropublication Biol*, **2020**, <https://doi.org/10.17912/micropub.biology.000315>.
121. Aalto, A.P., Nicastro, I.A., Broughton, J.P., Chipman, L.B., Schreiner, W.P., Chen, J.S. and Pasquinelli, A.E. (2018) Opposing

- roles of microRNA argonautes during *Caenorhabditis elegans* aging. *PLoS Genet.*, **14**, e1007379.
122. Martin, M. (2011) Cutadapt removes adapter sequences from high-throughput sequencing reads. *EMBnet.journal*, **17**, 10–12.
 123. Langmead, B., Trapnell, C., Pop, M. and Salzberg, S.L. (2009) Ultrafast and memory-efficient alignment of short DNA sequences to the human genome. *Genome Biol.*, **10**, R25.
 124. Danecek, P., Bonfield, J.K., Liddle, J., Marshall, J., Ohan, V., Pollard, M.O., Whitwham, A., Keane, T., McCarthy, S.A., Davies, R.M., et al. (2021) Twelve years of SAMtools and BCFtools. *Gigascience*, **10**, giab008.
 125. Anders, S., Pyl, P.T. and Huber, W. (2015) HTSeq—A Python framework to work with high-throughput sequencing data. *Bioinformatics*, **31**, 166–169.
 126. Love, M.I., Huber, W. and Anders, S. (2014) Moderated estimation of fold change and dispersion for RNA-seq data with DESeq2. *Genome Biol.*, **15**, 550.
 127. Kim, D., Paggi, J.M., Park, C., Bennett, C. and Salzberg, S.L. (2019) Graph-based genome alignment and genotyping with HISAT2 and HISAT-genotype. *Nat. Biotechnol.*, **37**, 907–915.
 128. Liao, Y., Smyth, G.K. and Shi, W. (2014) featureCounts: an efficient general purpose program for assigning sequence reads to genomic features. *Bioinformatics*, **30**, 923–930.
 129. Brown, K.C., Svendsen, J.M., Tucci, R.M., Montgomery, B.E. and Montgomery, T.A. (2017) ALG-5 is a miRNA-associated argonaute required for proper developmental timing in the *Caenorhabditis elegans* germline. *Nucleic Acids Res.*, **45**, 9093–9107.
 130. Vasquez-Rifo, A., Jannot, G., Armisen, J., Labouesse, M., Bukhari, S.I., Rondeau, E.L., Miska, E.A. and Simard, M.J. (2012) Developmental characterization of the microRNA-specific *C. elegans* argonautes alg-1 and alg-2. *PLoS One*, **7**, e33750.
 131. Kim, H., Kim, J., Kim, K., Chang, H., You, K.V. and Kim, N. (2019) Bias-minimized quantification of microRNA reveals widespread alternative processing and 3' end modification. *Nucleic Acids Res.*, **47**, 2630–2640.
 132. Alvarez-Saavedra, E. and Horvitz, H.R. (2010) Many families of *C. elegans* microRNAs are not essential for development or viability. *Curr. Biol.*, **20**, 367–373.
 133. Vieux, K.-F., Prothro, K.P., Kelley, L.H., Palmer, C., Maine, E.M., Veksler-Lublinsky, I. and McJunkin, K. (2021) Screening by deep sequencing reveals mediators of microRNA tailing in *C. elegans*. *Nucleic Acids Res.*, **49**, 11167–11180.
 134. Gu, S., Jin, L., Zhang, F., Huang, Y., Grimm, D., Rossi, J.J. and Kay, M.A. (2011) Thermodynamic stability of small hairpin RNAs highly influences the loading process of different mammalian Argonautes. *Proc. Natl. Acad. Sci. U.S.A.*, **108**, 9208–9213.
 135. Sheu-Gruttadauria, J., Pawlica, P., Klum, S.M., Wang, S., Yario, T.A., Schirle Oakdale, N.T., Steitz, J.A. and MacRae, I.J. (2019) Structural basis for target-directed MicroRNA degradation. *Mol. Cell*, **75**, 1243–1255.
 136. Yang, A., Shao, T.-J., Bofill-De Ros, X., Lian, C., Villanueva, P., Dai, L. and Gu, S. (2020) AGO-bound mature miRNAs are oligouridylated by TUTs and subsequently degraded by DIS3L2. *Nat. Commun.*, **11**, 2765.
 137. Khvorova, A., Reynolds, A. and Jayasena, S.D. (2003) Functional siRNAs and miRNAs exhibit strand bias. *Cell*, **115**, 209–216.
 138. Schwarz, D.S., Hutvagner, G., Du, T., Xu, Z., Aronin, N. and Zamore, P.D. (2003) Asymmetry in the assembly of the RNAi enzyme complex. *Cell*, **115**, 199–208.
 139. Medley, J.C., Panzade, G. and Zinovyeva, A.Y. (2021) microRNA strand selection: unwinding the rules. *Wiley Interdiscip. Rev. RNA*, **12**, e1627.
 140. Jan, C.H., Friedman, R.C., Ruby, J.G. and Bartel, D.P. (2011) Formation, regulation and evolution of *Caenorhabditis elegans* 3'UTRs. *Nature*, **469**, 97–101.
 141. Cazalla, D., Yario, T., Steitz, J.A. and Steitz, J. (2010) Down-regulation of a host microRNA by a herpesvirus saimiri noncoding RNA. *Science*, **328**, 1563–1566.
 142. de la Mata, M., Gaidatzis, D., Vitanescu, M., Stadler, M.B., Wentzel, C., Scheiffele, P., Filipowicz, W. and Grosshans, H. (2015) Potent degradation of neuronal miRNAs induced by highly complementary targets. *EMBO Rep.*, **16**, 500–511.
 143. Pawlica, P., Moss, W.N. and Steitz, J.A. (2016) Host miRNA degradation by Herpesvirus saimiri small nuclear RNA requires an unstructured interacting region. *RNA*, **22**, 1181–1189.
 144. Kingston, E.R. and Bartel, D.P. (2021) Ago2 protects drosophila siRNAs and microRNAs from target-directed degradation, even in the absence of 2-O-methylation. *RNA*, **27**, 710–724.
 145. Kingston, E.R., Blodgett, L.W. and Bartel, D.P. (2022) Endogenous transcripts direct microRNA degradation in *Drosophila*, and this targeted degradation is required for proper embryonic development. *Mol. Cell*, **82**, 3872–3884.
 146. Ameres, S.L., Horwich, M.D., Hung, J.-H., Xu, J., Ghildiyal, M., Weng, Z. and Zamore, P.D. (2010) Target RNA-directed trimming and tailing of small silencing RNAs. *Science*, **328**, 1534–1539.
 147. Libri, V., Helwak, A., Miesen, P., Santhakumar, D., Borger, J.G., Kudla, G., Grey, F., Tollervey, D. and Buck, A.H. (2012) Murine cytomegalovirus encodes a miR-27 inhibitor disguised as a target. *Proc. Natl. Acad. Sci. U.S.A.*, **109**, 279–284.
 148. Marcinowski, L., Tanguy, M., Krmpotic, A., Rädle, B., Lisnić, V.J., Tuddenham, L., Chane-Woon-Ming, B., Ruzsics, Z., Erhard, F., Benkartek, C., et al. (2012) Degradation of cellular mir-27 by a novel, highly abundant viral transcript is important for efficient virus replication in vivo. *PLoS Pathog.*, **8**, e1002510.
 149. Lee, S., Song, J., Kim, S., Kim, J., Hong, Y., Kim, Y., Kim, D., Baek, D. and Ahn, K. (2013) Selective degradation of host MicroRNAs by an intergenic HCMV noncoding RNA accelerates virus production. *Cell Host Microbe*, **13**, 678–690.
 150. Ghini, F., Rubolino, C., Climent, M., Simeone, L., Marzi, M.J. and Nicassio, F. (2018) Endogenous transcripts control miRNA levels and activity in mammalian cells by target-directed miRNA degradation. *Nat. Commun.*, **9**, 3119.
 151. Bitetti, A., Mallory, A.C., Golini, E., Carrieri, C., Carreño Gutiérrez, H., Perlas, E., Pérez-Rico, Y.A., Tocchini-Valentini, G.P., Enright, A.J., Norton, W.H.J., et al. (2018) MicroRNA degradation by a conserved target RNA regulates animal behavior. *Nat. Struct. Mol. Biol.*, **25**, 244–251.
 152. Kleaveland, B., Shi, C.Y., Stefano, J. and Bartel, D.P. (2018) A network of noncoding regulatory RNAs acts in the mammalian brain. *Cell*, **174**, 350–362.
 153. Li, L., Sheng, P., Li, T., Fields, C.J., Hiers, N.M., Wang, Y., Li, J., Guardia, C.M., Licht, J.D. and Xie, M. (2021) Widespread microRNA degradation elements in target mRNAs can assist the encoded proteins. *Genes Dev.*, **35**, 1595–1609.
 154. Han, J., LaVigne, C.A., Jones, B.T., Zhang, H., Gillett, F. and Mendell, J.T. (2020) A ubiquitin ligase mediates target-directed microRNA decay independently of tailing and trimming. *Science*, **370**, eabc9546.
 155. Shi, C.Y., Kingston, E.R., Kleaveland, B., Lin, D.H., Stubna, M.W. and Bartel, D.P. (2020) The ZSWIM8 ubiquitin ligase mediates target-directed microRNA degradation. *Science*, **370**, eabc9359.
 156. Wang, Z., Hou, Y., Guo, X., vander Voet, M., Boxem, M., Dixon, J.E., Chisholm, A.D. and Jin, Y. (2013) The EBAX-type cullin-RING E3 ligase and Hsp90 guard the protein quality of the SAX-3/robo receptor in developing neurons. *Neuron*, **79**, 903–916.
 157. Donnelly, B.F., Yang, B., Grimme, A.L., Vieux, K.F., Liu, C.Y., Zhou, L. and McJunkin, K. (2022) The developmentally timed decay of an essential microRNA family is seed-sequence dependent. *Cell Rep.*, **40**, 111154.
 158. Buntru, M., Vogel, S., Stoff, K., Spiegel, H. and Schillberg, S. (2015) A versatile coupled cell-free transcription–translation system based on tobacco BY-2 cell lysates. *Biotechnol. Bioeng.*, **112**, 867–878.

159. Nakanishi,K. (2023) When Argonaute takes out the ribonuclease sword. *J. Biol. Chem.*, **300**, 105499.
160. Gu,S., Jin,L., Huang,Y., Zhang,F. and Kay,M.A. (2012) Slicing-independent RISC activation requires the argonaute PAZ domain. *Curr. Biol.*, **22**, 1536–1542.
161. Chatterjee,S., Fasler,M., Büssing,I. and Grosshans,H. (2011) Target-mediated protection of endogenous microRNAs in *C. elegans*. *Dev. Cell*, **20**, 388–396.
162. Czech,B. and Hannon,G.J. (2016) One loop to rule them all: the ping-pong cycle and piRNA-guided silencing. *Trends Biochem. Sci.*, **41**, 324–337.